Journal of Comparative Neurology

WILEY

JCN RESEARCH IN SYSTEMS NEUROSCIENCE THE JOURNAL OF COMPARATIVE NEUROLOGY

RESEARCH ARTICLE OPEN ACCESS

Immature Excitatory Neurons in the Postnatal Ferret Paralaminar Nuclei and Their Relationship to the Amygdala Across Species

Lucía Inés Torrijos-Saiz[1] | Marco Ghibaudi[2] | Malaz Sharief[2] | Lovisa Ljungqvist Brinson[3,4,5] | Arturo Alvarez-Buylla[6,7] | José Manuel García-Verdugo[1] | Vicente Herranz-Pérez[8] | Shawn Sorrells[2,5,9]

[1]Laboratory of Comparative Neurobiology, Cavanilles Institute of Biodiversity and Evolutionary Biology, University of Valencia—CIBERNED-ISCIII, Paterna, Spain | [2]Department of Neuroscience, University of Pittsburgh, Pittsburgh, Pennsylvania, USA | [3]Department of Neurobiology, University of Pittsburgh, Pittsburgh, Pennsylvania, USA | [4]Center for Neuroscience, University of Pittsburgh, Pittsburgh, Pennsylvania, USA | [5]Center for the Neural Basis of Cognition, University of Pittsburgh, Pittsburgh, Pennsylvania, USA | [6]Eli and Edythe Broad Institute for Stem Cell Research and Regeneration Medicine, University of California, San Francisco, California, USA | [7]Department of Neurological Surgery, University of California, San Francisco, California, USA | [8]Department of Cellular Biology, Functional Biology and Physical Anthropology, University of Valencia—CIBERNED-ISCIII, Burjassot, Spain | [9]Department of Neurological Surgery, University of Pittsburgh, Pittsburgh, Pennsylvania, USA

Correspondence: Vicente Herranz-Pérez (vicente.herranz@uv.es) | Shawn Sorrells (shawn.sorrells@pitt.edu)

Received: 22 September 2025 | **Revised:** 17 February 2026 | **Accepted:** 14 March 2026

Keywords: amygdala | ferret | gyrencephalic mammals | immature neurons | neuronal migration | paralaminar nuclei | postnatal development

ABSTRACT

The amygdala paralaminar nuclei (PL) contain immature excitatory neurons that develop on a delayed timeline from birth to adulthood and are more prominent in the amygdala of humans and other primates than in rodents. Whether this expansion is linked to brain complexity or is a feature of primates is unknown. We sought to identify the PL in the ferret (*Mustela putorius furo*), a small, gyrencephalic mammal that does not belong to the primate order. Here, we show that the amygdala of juvenile (P30–P67) and adult ferrets (>1 year) also contains a collection of immature excitatory neurons that express doublecortin (Dcx) and polysialylated neural cell adhesion molecule (Psa-Ncam). Similar to humans and mice, these immature neurons express Tbr1 and CoupTFII, but not FoxP2, which labels neighboring clusters of GABAergic cells in the intercalated nuclei. Ferret PL neurons extend into the ventral basolateral amygdala (BLA) and appear either in dense clusters surrounded by astroglia or as individual cells, and each subpopulation contains neurons with migratory morphology. This expansion of PL neurons into the amygdala is

Abbreviations: 3V, third ventricle; A, astrocyte; AA, anterior amygdaloid area; ACo, cortical amygdala; AEG, agranular insular area; AHi, amygdalohippocampal area; Amyg, amygdala; ASG, anterior sigmoid gyrus; ASt, amygdalostriatal transition area; BA, basal amygdala; BLA, basolateral amygdala; BLV, ventral basolateral amygdala; BMA, basomedial amygdala; BMP, posterior basomedial nucleus; CA1, cornu ammonis 1; CA3, cornu ammonis 3; CeA, central amygdala; Cl, claustrum; CNG, coronal gyrus; CoupTFII, chicken ovalbumin upstream promoter transcription factor II; Ctip2, CoupTF interacting protein 2; CxA, amygdaloid cortex; DAPI, 4′,6-diamidino-2-phenylindole; Dcx, doublecortin; DEn, dorsal endopiriform cortex; DG, dentate gyrus; DMSO, dimethyl sulfoxide; ec, external capsule; FoxP2, forkhead box protein 2; GCL, granule cell layer; GFAP, glial fibrillary acidic protein; HC, hippocampus; I, intercalated nuclei; IF, immunofluorescence; IHC, immunohistochemistry; iN, immature neuron; LA, lateral amygdala; LEnt, lateral entorhinal cortex; lot, lateral olfactory tract; LPL, lateral paralaminar nuclei; LV, lateral ventricle; MeA, medial amygdala; MEnt, medial entorhinal cortex; MPL, medial paralaminar nucleus; NeuN, neuronal nuclear antigen; NGS, normal goat serum; OL, oligodendrocyte; PaS, parasubiculum; PBS, phosphate-buffered saline; PFA, paraformaldehyde; PirCx, piriform cortex; PL, paralaminar nuclei; PLCo, posterolateral cortical nucleus of the amygdala; PMCo, posteromedial cortical nucleus of the amygdala; PrS, presubiculum; Psa-Ncam, polysialylated neural cell adhesion molecule; PSG, posterior sigmoid gyrus; S, subiculum; Satb2, special AT-rich sequence-binding protein 2; SGZ, subgranular zone; Sox11, SRY-box transcription factor 11; Tbr1, T-box brain transcription factor 1; TEM, transmission electron microscopy; VEn, ventral endopiriform cortex; V-SVZ, ventricular-subventricular zone; wm, white matter.

Vicente Herranz-Pérez and Shawn Sorrells contributed equally to this study.

similar to what is seen in humans, but unlike in mice, where PL neurons are infrequent in the BLA. We compared these findings to the marmoset (*Callithrix jacchus*), a lissencephalic non-human primate, and the swine (*Sus scrofa domesticus*), a gyrencephalic mammal, and found immature neurons extending into the amygdala in both. Our study identifies the PL region of the ferret amygdala, which contains immature neurons with migratory features in juveniles and adults. Cross-species comparisons indicate that the expansion of PL neurons into the amygdala seen in primates with both high and low gyrencephalic indices has also occurred in species with gyrencephalic brains from different orders.

1 | Introduction

The amygdala is a complex and specialized brain region involved in emotional learning and behavior. It is composed of strongly inter- and intraconnected nuclei generated during embryonic stages (Aerts and Seuntjens 2021) that reach a mature cytoarchitectonical appearance before birth in mammals ranging from mice to humans (McConnell and Angevine 1983; Soma et al. 2009; Remedios et al. 2007; Mulc et al. 2024).

The paralaminar nuclei (PL) of the amygdala are composed of a large population of small, densely packed cells. This region can be identified by a high density of cell nuclei expressing the transcription factors Tbr1, CoupTFII, and Ctip2 (Alderman et al. 2024; Sorrells et al. 2019). First described in humans (Crosby and Humphrey 1941), the PL is present in many species with different brain features and complexities, such as rats (Flügge et al. 1994), tree shrews (Ai et al. 2021), cats (Amaral and Price 1984; Martí-Mengual et al. 2013), microchiropterans (Chawana et al. 2016), and non-human primates (Bernier et al. 2002; Fasemore et al. 2018; Zhang et al. 2009; Marlatt et al. 2011). The PL is particularly prominent in primates compared to other mammals, containing more cells than the surrounding amygdala nuclei and occupying more space along the basolateral amygdala (BLA) complex (deCampo and Fudge 2012; Chareyron et al. 2011; Sorrells et al. 2019; Page et al. 2022; Chareyron et al. 2021).

Although the birth of its neurons occurs during embryonic stages along with the rest of the amygdaloid complex, the PL exhibits a delayed developmental timeline. Its protracted development results from the growth of immature excitatory neurons that undergo molecular and morphological maturation primarily during postnatal life (Alderman et al. 2024; Sorrells et al. 2019; Li et al. 2023; Chareyron et al. 2021; Marlatt et al. 2011; Martí-Mengual et al. 2013; Zhang et al. 2009). Therefore, the PL contains different subpopulations of immature excitatory neurons at different maturational stages. The most immature have small somas with compacted chromatin and few organelles, whereas others appear more mature, with larger somas, ramified dendrites, and more organelles (Alderman et al. 2024; Sorrells et al. 2019; deCampo and Fudge 2012). Immature PL cells can be detected by the expression of common markers of young neurons, such as doublecortin (Dcx), a microtubule-associated protein crucial for correct cortical layer formation, whose expression is high in migrating young neurons and is then downregulated during final differentiation (Gleeson et al. 1999; Brown et al. 2003), and the polysialylated form of the neural cell adhesion molecule (Psa-Ncam), which is widely distributed in the developing nervous system where it promotes dynamic cell–cell interactions (Bonfanti and Theodosis 2009). Quantifications of Dcx and Psa-Ncam expression indicate that the number of immature excitatory neurons significantly declines between birth and adulthood, leaving a small reservoir of immature cells in adults, both in mice and humans (Alderman et al. 2024; Sorrells et al. 2019).

Prior comparative analysis revealed differences in the association of the PL with the BLA between species with differing brain gyrification and complexity. In some species with small, lissencephalic brains like mice and bats, the PL is located rostral to the BLA (Alderman et al. 2024; Chawana et al. 2016). A, subset of the immature PL neurons in mice appear migratory and are primarily observed extending into the ventral endopiriform cortex (Alderman et al. 2024). In gyrencephalic species with larger brains, such as cats and primates (including humans), the PL is present along a large rostral-caudal boundary of the BLA (Martí-Mengual et al. 2013; Zhang et al. 2009; Sorrells et al. 2019). Interestingly, however, some lissencephalic animals more closely related to humans, such as the tree shrew (Ai et al. 2021) and marmoset (Marlatt et al. 2011; Ghibaudi et al. 2025), also have this larger PL association with the BLA, raising the question of how this association evolved.

To investigate the phylogenetic divergence of PL association with the amygdala, we selected several mammals for this study. The ferret (*Mustela putorius furo)* is from a different placental clade than humans or mice, and it has a relatively small gyrencephalic brain (Lockard 1985). The ferret also has an extended postnatal brain development, with sulcal and gyral folds emerging during the first 28 postnatal days (Ellis et al. 2019; Barnette et al. 2009; Sawada and Watanabe 2012). We also compared the PL association with the amygdala in humans (*Homo sapiens*), mice (*Mus musculus*) which have previously been studied (Martì–Mengual et al., 2013; Avino et al., 2018; Alderman et al. 2024; Sorrells et al. 2019), the common marmoset (*Callithrix jacchus*), a species with a small, lissencephalic brain but nuclear subdivisions and fiber tracts of the amygdala resembling those in humans and macaques (A. G. Morais et al. 2019), and the swine (*Sus scrofa domesticus*), a mammal with a large and rapidly developing gyrencephalic brain that shares important developmental and anatomical features with humans, including a prolonged period of postnatal maturation (Conrad et al. 2012).

Here, we show that ferrets have a homologous PL region that is highly associated with the amygdala and contains dense collections of immature excitatory neurons, many of which exhibit morphological and molecular features of migratory neurons. Comparison with marmoset and swine revealed that these species also have a homologous PL region, providing further evidence

that the delayed maturation of these nuclei is a conserved feature across mammals.

2 | Methods

2.1 | Animals

All animal procedures and experimental protocols were approved by the Institutional Animal Care and Use Committee (IACUC) at The University of Pittsburgh or the University of California, San Francisco (UCSF), and were conducted in accordance with NIH guidelines for animal research. Human postmortem tissue was collected with and in accordance with institutional guidelines and with study design approval by the Committee for Oversight of Research and Clinical Training Involving Decedents (CORID) at the University of Pittsburgh or the UCSF Committee on Human Research.

2.1.1 | Mouse

All experiments were conducted in accordance with approved protocols by the University of Pittsburgh IACUC and following NIH guidelines for animal research. Male and female C57Bl/6J (Jackson Labs, Strain #: 000664) wildtype mice used in this study were socially housed (up to four mice/cage) on a 12-h day/night cycle with ad libitum food and water in a pathogen-free facility. All mice used in this study were healthy, used only as described for each experiment (Table 1), and did not undergo prior experimental procedures.

2.1.2 | Human

We collected tissue blocks from the temporal lobe, anteriorly from the amygdaloid complex to the posterior end of the inferior horn of the lateral ventricle. Samples were fixed in 4% paraformaldehyde (PFA) for >24 h. Brains were cut into ~1.5 cm blocks, cryoprotected in a series of 10%, 20%, and 30% sucrose solutions, and then frozen in OCT embedding medium. Blocks of the medial temporal lobe were cut into 20 μm thick sections on a cryostat (Leica CM3050S) and mounted on glass slides for immunohistochemistry (Table 1). The 15-year-old sample was male with a clinical history of acute lymphoblastic leukemia and 22 h postmortem interval (PMI). The 24-year-old sample was female with a clinical history of acute kidney injury and multiorgan failure, and 16 h PMI. Neither case had detectable neuropathology.

2.1.3 | Ferret

Pregnant ferrets (*M. putorius furo*) at embryonic day 26 (E26) were obtained from Marshall Farms (North Rose, NY). Juvenile or adult ferrets were terminally anesthetized with an isoflurane vaporizer and perfused transcardially with 0.1 M phosphate-buffered saline (PBS; pH 7.4), followed by 4% PFA in PBS (pH 7.4). Brains were removed from the skull and post-fixed overnight in 4% PFA at 4°C. Following fixation, brains were cryoprotected in 30% sucrose in 0.1 M PBS until they sank. For sectioning, brains were frozen onto the stage of a sliding microtome (Leica SM2010R), and 50 μm floating sections were cut in coronal, sagittal, and horizontal planes. Sections were stored in 6-well cell culture plates containing 0.1 M PBS with sodium azide at 4°C and subsequently used for free-floating immunohistochemistry (Table 1). To identify ferret anatomical structures, we used "Cyto- and Myeloarchitectural Brain Atlas of the Ferret (*Mustela putorius*) in MRI Aided Stereotaxic Coordinates" (Radtke-Schuller 2018).

2.1.4 | Marmoset

A 3-year-old male marmoset brain (*C. jacchus*) was obtained from the University of Pittsburgh Systems Neuroscience Animal Research Laboratory (SNARL) colony (Table 1). The subject was housed in an AAALAC-accredited facility at the University of Pittsburgh and maintained at a temperature range of 24.4–25.6°C and 30%–70% humidity, with a 12 h:12 h light/dark cycle (lights on at 7 a.m.). The subject was socially housed with a compatible cage-mate during adulthood and was fed an ad libitum diet with unrestricted water access, while also being provided with toys and enrichment items. The marmoset was anesthetized with ketamine (30 mg/kg, intramuscular), followed by euthanasia via an overdose of pentobarbital (100 mg/kg, intraperitoneal). After confirming the absence of reflexes, the thoracic cavity was opened, and transcardial perfusion–fixation was performed using a peristaltic pump with 0.1 M PBS. Liver coloration was monitored throughout perfusion to ensure complete exsanguination and adequate fixation. Following perfusion, the brain was removed and the hemispheres were separated. The hemisphere used for this study was post-fixed in 4% PFA and stored in a 4°C refrigerator for 72 h. Afterward, they were placed in a 30% sucrose solution in 0.1 M PBS until they sank for cryoprotection. The hemisphere was frozen in a plastic tray with embedding medium (OCT), removed, frozen to a removable cryostat puck, and allowed to temperature-stabilize in the cryostat for 30–60 min (Leica CM1950). Sagittal sections (30 μm thick) were sliced and stored in 6-well cell culture plates containing 30% sucrose (Liu et al. 2021).

2.1.5 | Swine

Swine brain samples (*S. scrofa domesticus*) were obtained from the Center of Applied Biomedical Experimental Research (CREBA) in Lleida, Spain. The animals had been previously used in non-survival surgical procedures unrelated to the brain, conducted under anesthesia with continuous veterinary supervision, in compliance with European Union and Spanish government regulations (BOE-A-2013-1337). Animals were euthanized with a lethal dose of sodium pentobarbital, after which brains were extracted, and the hemispheres were fixed by immersion in 4% PFA in 0.1 M phosphate buffer (PB) for 72 h at 4°C. Following fixation, brains were rinsed with 0.1 M PB and stored in the same buffer containing 0.05% sodium azide at 4°C. One hemisphere from each brain was cryoprotected and stored at −80°C for subsequent sectioning with a freezing microtome. Cryoprotection involved sequential immersion at 4°C in a 10% glycerol and 2% dimethyl sulfoxide (DMSO) solution in 0.1 M PB overnight, followed by immersion in a 20% glycerol and 2% DMSO solution in 0.1 M PB for 48 h. The brains were rapidly frozen by immersion in −75°C isopentane for 5 min. The contralateral hemispheres

TABLE 1 | Animals, ages, and experimental use.

#	Species	Age	Fixation	Sectioning	Experimental use	Orientation
1	*Mustela putorius furo*	P10	4% PFA	50 μm sliding microtome	IHC	Coronal and sagittal
2	*Mustela putorius furo*	P10	4% PFA	50 μm sliding microtome	IHC	Coronal and sagittal
3	*Mustela putorius furo*	P30	4% PFA	50 μm sliding microtome	IHC	Coronal and sagittal
4	*Mustela putorius furo*	P40	4% PFA	50 μm sliding microtome	IHC	Coronal
5	*Mustela putorius furo*	P40	4% PFA	50 μm sliding microtome	IHC	Coronal
6	*Mustela putorius furo*	P40	4% PFA	50 μm sliding microtome	IHC	Coronal
7	*Mustela putorius furo*	P40	4% PFA	50 μm sliding microtome	IHC	Coronal
8	*Mustela putorius furo*	P40	4% PFA	50 μm sliding microtome	IHC	Coronal
9	*Mustela putorius furo*	P42	4% PFA	20 μm cryostat	IHC	Coronal
10	*Mustela putorius furo*	P47	2% PFA, 2.5% Gluta	200 μm vibratome	TEM	Coronal
11	*Mustela putorius furo*	P65	4% PFA	50 μm sliding microtome	IHC	Coronal and sagittal
12	*Mustela putorius furo*	P65	4% PFA	50 μm sliding microtome	IHC	Coronal and sagittal
13	*Mustela putorius furo*	P65	ZnS	50 μm sliding microtome	Timm's stain	Coronal
14	*Mustela putorius furo*	P66	2% PFA, 2.5% Gluta	200 μm vibratome	TEM	Coronal
15	*Mustela putorius furo*	P66	4% PFA	50 μm sliding microtome	IHC	Coronal
16	*Mustela putorius furo*	P67	4% PFA	50 μm sliding microtome	IHC	Sagittal
17	*Mustela putorius furo*	Adult (1.3 years)	4% PFA	50 μm sliding microtome	IHC	Coronal and sagittal
18	*Mustela putorius furo*	Adult (1.3 years)	4% PFA	50 μm sliding microtome	IHC	Coronal and sagittal
19	*Mustela putorius furo*	Adult (1.3 years)	2% PFA, 2.5% Gluta	200 μm vibratome	TEM	Coronal
20	*Mus musculus*	Adult (P60)	4% PFA	50 μm sliding microtome	IHC	Sagittal
21	*Sus scrofa domesticus*	4 months	4% PFA	100 μm sliding microtome and 200 μm vibratome	IHC	Coronal and sagittal
22	*Sus scrofa domesticus*	5 months	4% PFA	100 μm sliding microtome and 200 μm vibratome	IHC	Coronal and sagittal
23	*Callithrix jacchus*	3 years	4% PFA	30 μm cryostat	IHC	Sagittal
24	*Homo sapiens*	15 years	4% PFA	20 μm cryostat	IHC	Sagittal
25	*Homo sapiens*	24 years	4% PFA	20 μm cryostat	IHC	Coronal

Abbreviations: Gluta, glutaraldehyde; IHC, immunohistochemistry; PFA, paraformaldehyde; TEM, transmission electron microscopy.

TABLE 2 | Primary antibodies.

Antigen	Species	Dilution	Use	Manufacturer, reference, RRID	Specificity
CoupTFII	Mouse	1:250	IF	R&D Systems, Cat# PP-H7147-00, RRID: AB_2155627	Excitatory neurons
Ctip2	Rat	1:250	IF	Abcam, Cat# ab18465, RRID: AB_2064130	Excitatory neurons
Dcx	Rabbit	1:200	IHC, IF	Cell Signaling Technology, Cat# 4604, RRID: AB_561007	Immature neurons
Dcx	Rabbit	1:100	IG-Au	Cell Signaling Technology, Cat# 4604, RRID: AB_561007	Immature neurons
FoxP2	Goat	1:500	IF	Santa Cruz Biotechnology, Cat# 517261; lot # G2216; RRID:AB_2721204	Inhibitory neurons
GFAP	Mouse	1:500	IF	EMD Millipore Cat# Z0334; lot # 3194598; RRID:AB_10013382	Astrocytes
GFAP	Chicken	1:1000	IF	Millipore, Cat# AB5541, RRID: AB_177521	Astrocytes
NeuN	Chicken	1:500	IF	Millipore, Cat# ABN91, RRID: AB_11205760	Mature neurons
Psa-Ncam IgM	Mouse	1:250	IF	Millipore, Cat# MAB5324, RRID: AB_95211	Immature migrating neurons
Sox11	Rabbit	1:250	IF	Millipore, Cat# AB5776 RRID: AB_2195196	Immature migrating neurons
Tbr1	Chicken	1:200	IF	Millipore, Cat# AB2261, RRID: AB_10615497	Excitatory neurons

Abbreviations: IF, immunofluorescence; IG-Au, immunogold labeling for transmission electron microscopy; IHC, immunohistochemistry.

were sectioned with a vibratome (VT1200S vibratome [Leica Microsystems]) (Table 1).

2.2 | Immunofluorescence Staining

For immunofluorescence, tissue fixed in 4% PFA was sectioned into either 50 or 100 μm floating sections or 10 μm paraffin sections. Sections were rinsed in 0.1 M PB, and endogenous peroxidase activity was blocked with 3% H_2O_2 and 10% methanol in 0.1 M PB. Antigen retrieval was performed by incubating sections in Immunosaver (64142; Electron Microscopy Sciences) for 30 min at 60°C. After washing in PTA (0.1% Triton X-100 and 0.1% bovine serum albumin [BSA] in 0.1 M PB), sections were incubated for 1 h in a blocking solution containing 10% casein and 5% normal goat serum (NGS) in PTA. Primary antibodies (Table 2) were diluted in blocking solution and incubated overnight at 4°C. After washing with PTA, sections were incubated with secondary antibodies (Table 3) diluted in blocking solution for 1 h at room temperature. Sections were rinsed in 0.1 M PB and incubated for 10 min with 4′,6-diamino-2-phenylindol (DAPI; 1:1000 dilution in dH_2O) to label cell nuclei. Finally, sections were mounted using FluorSave (Millipore). Confocal images were collected using either a Leica TCS SP8 microscope (Leica Microsystems, Wetzlar, Germany) or an Olympus FV1000 confocal microscope. For Dcx GFAP coexpression, image deconvolution was performed using the Lightning function on Leica TCS SP8 software.

2.3 | Timm's Stain

Timm's staining was performed following the manufacturer's specifications (FD Neurotech, PK701). First, the tissue sections were washed three times for 3 min each in 0.1 M PB (pH 7.4). Next, sections were incubated for 50 min at 30°C in the dark in a freshly prepared staining solution composed of Solutions A, B, C, and D (for a 100 mL solution: 40 mL of solution A + 30 mL of solution B + 30 mL of solution C + 10 drops of solution D). Color development was monitored under a microscope after 30 min of incubation, and the incubation time was adjusted as needed to control staining intensity. To stop the reaction, sections were transferred to distilled water, then rinsed in double-distilled or Milli-Q water for 3 min in the dark. Subsequently, sections were washed gently in running water for 30 min, minimizing exposure to light. Next, they were rinsed again in distilled water for 3 min before sequential dehydration in 50%, 75%, and 95% ethanol for 3 min each. Finally, sections were dehydrated in absolute ethanol and cleared in xylene or a xylene substitute three times for 3 min each and mounted with a resinous medium for preservation and imaging.

TABLE 3 | Secondary antibodies.

Antibody	Species	Dilution	Use	Manufacturer, reference, RRID
Anti-chicken Alexa 647	Goat	1:300	IF	Abcam, Cat# ab150175, RRID: AB_2732800
Anti-goat IgG (H + L) Alexa 488	Donkey	1:500	IF	Jackson ImmunoResearch, Cat# 705-546-147, RRID: AB_2340430
Anti-mouse Alexa 488	Goat	1:300	IF	Molecular Probes, Cat# A-21424, RRID: AB_141780
Anti-rabbit (H + L) Alexa 555	Goat	1:300	IF	Molecular Probes, Cat# A-21428, RRID: AB_141784
Anti-rabbit biotinylated	Goat	1:300	IHC	Vector Laboratories, Cat# BA-1000, RRID: AB_2313606
Anti-rabbit gold 10 nm	Goat	1:50	IG-Au	Sigma-Aldrich, Cat# G7402, RRID: AB_259953
Anti-rat IgG (H + L) Alexa 405	Goat	1:250	IF	Invitrogen, Cat# A48261; RRID: AB_2890550

Abbreviations: IF, immunofluorescence; IG-Au, immunogold labeling for transmission electron microscopy; IHC, immunohistochemistry.

2.4 | Pre-Embedding Immunogold Labeling

Free-floating coronal sections (50 μm thick) were cut from brains fixed in 4% PFA using a Leica VT1200S vibratome (Leica Microsystems). Sections were cryoprotected in 25% sucrose in 0.1 M PB for 30 min, then subjected to freeze–thaw cycles in methylbutane at −60°C to enhance permeabilization. After rinsing in 0.1 M PB, sections were incubated for 1 h at room temperature in blocking solution (0.3% BSAc and 0.05% sodium azide in 0.1 M PB). Primary antibodies (Table 2) were diluted in blocking solution and applied for 96 h at 4°C. Following washes in 0.1 M PB, sections were incubated for 1 h at room temperature in a secondary blocking solution (0.5% BSAc and 0.1% fish gelatin in 0.1 M PB) and then exposed to colloidal gold-conjugated secondary antibodies (0.8 nm; Aurion) (Table 3) for 24 h at 4°C. After washing in 0.1 M PB, sections were rinsed in 2% sodium acetate in distilled water. Silver enhancement was performed using a commercial kit (Aurion) to amplify the immunogold signal. Sections were then rinsed again in 2% sodium acetate and treated with 0.05% gold chloride in distilled water for 10 min at 4°C to stabilize silver particles. A final rinse in 0.03% sodium thiosulfate and 0.1 M PB was performed prior to post-fixation in 2% glutaraldehyde in 0.1 M PB for 30 min, followed by thorough washes in 0.1 M PB. Dehydration, resin embedding, ultrathin sectioning, and image acquisition were performed according to the procedures described in Section 2.5.

2.5 | Conventional Transmission Electron Microscopy

Sagittal sections (100 μm thick) were cut with a Leica VT1200S vibratome (Leica Microsystems) from samples fixed in 2% PFA and 2.5% glutaraldehyde in 0.1 M PB. Sections were incubated in 2% osmium tetroxide (Electron Microscopy Sciences) in 0.1 M PB for 1 h 30 min at room temperature. For immunogold labeling, incubation was performed in 1% osmium tetroxide and 7% glucose in 0.1 M PB for 30 min to minimize gold particle masking. After thorough rinsing in deionized water, sections were partially dehydrated through graded ethanol (30%, 50%, 70%) and contrasted in 2% uranyl acetate (Electron Microscopy Sciences) in 70% ethanol for 2 h at 4°C. They were then further dehydrated through ascending ethanol concentrations (70%, 90%, 100%) and infiltrated with Durcupan ACM epoxy resin (Fluka, Sigma-Aldrich) at room temperature overnight. The following day, samples were transferred to fresh resin. Polymerization was carried out at 60°C for 72 h. The polymerized blocks were trimmed to the region of interest and sectioned into semithin (1.5 μm) and ultrathin (60–80 nm) sections using a UC7 ultramicrotome (Leica Biosystems). Ultrathin sections were mounted on Formvar-coated single-slot copper grids (Electron Microscopy Sciences), stained with lead citrate, and examined at 80 kV in an FEI Tecnai G^2 Spirit transmission electron microscope (FEI Company, Hillsboro, OR) equipped with a XAROSA CMOS digital camera (EMSIS GmbH).

2.6 | Quantifications and Statistical Analysis

Amygdala/Dcx^+ cell overlap analysis was performed on juvenile (P40, P66) and adult (1.3 years) ferrets (three individuals/age). Briefly, three representative levels at the anterior, middle, and posterior portions of the amygdala/PL were selected for each individual. At each level, both the amygdala and Dcx^+ cell areas were traced using a 10× objective and Stereoinvestigator Software (MBF Bioscience). The amygdala/Dcx^+ cells overlap area was then measured for each section using the Cavalieri estimator probe in Stereoinvestigator Software, with the following parameters: grid size, 100 μm; section thickness, 50 μm; randomized rotation. The mean % of the amygdala/Dcx^+ cells overlap area (% obtained by dividing the amygdala/Dcx^+ cells overlap area/amygdala area × 100) and the mean sum of the amygdala/Dcx^+ cells overlap area (mm^2) are reported in Table 4.

Soma elongation index (SEI) analysis was performed on 40× confocal acquisitions of Dcx^+ cells at juvenile (P40, P66) and adult (1.3 years) ferrets. Briefly, both Dcx^+ cells' soma primary (long) axis and orthogonal to the primary axis (short axis) were traced using ImageJ software (Wayne Rasband at the National Institutes of Health) and measured using the "Analyze—Measure" function on ImageJ. SEI was then obtained using the following formula: short axis/long axis. The area of each Dcx^+ cell was calculated using the ellipsoid method. Briefly, the short axis (Dx) and long axis (Dy) were considered cell diameters, and the radii (*a, b*)

TABLE 4 | Dcx^+ cells/amygdala overlap analysis data in the juvenile and adult ferret.

Age	Cavalieri Probe Mean sum ± *SD* Dcx^+ cells/amygdala overlap area (mm^2)	Cavalieri Probe Mean % ± *SD* Dcx^+ cells/amygdala overlap
P40	1.89 ± 0.66	16.67 ± 2.90
P66	0.80 ± 0.31	4.55 ± 0.73
Adult	0.91 ± 0.10	8.60 ± 2.52

for each axis were measured (a = Dx/2 and b = Dy/2). The final area was then calculated using the geometrical formula for ellipsoids: $A = \pi ab$. As the number of animals was not sufficient to perform statistical analysis, we provide descriptive statistics for SEI analysis. For elongated cells, at P40 (n = 17, range = 0.4, mean = 0.5, SD = 0.1), P66 (n = 18, range = 0.4, mean = 0.5, SD = 0.1), and adult (n = 18, range = 0.3, mean = 0.5, SD = 0.08). For rounded cells, at P40 (n = 84, range = 1.0, mean = 0.9, SD = 0.1), P66 (n = 82, range = 0.8, mean = 0.8, SD = 0.1), and adult (n = 85, range = 0.6, mean = 0.8, SD = 0.1).

Dcx^+/$NeuN^+$ cell quantifications were performed on adult mouse (P60), marmoset (3 years), ferret (1.3 years), and human (24 years) PL (one individual/species). Briefly, three representative sections at the anterior, middle, and posterior parts of the amygdala/PL were stained for Dcx and NeuN in all species (one section/level). Three confocal fields at 10×/0.45 were then acquired along the PL and analyzed on Stereoinvestigator Software (nine confocal fields/individual): The total number of $Dcx^+$and $NeuN^+$ cells and PL area were collected, and the $Dcx^+$and $NeuN^+$ cell density (cell/mm^2) and the % of Dcx^+NeuN^+ cells out of the total Dcx^+ cell population were determined.

Molecular marker co-expression analysis was performed at different developmental stages by quantifying Tbr1 and CoupTFII expression. Quantifications were performed using Fiji. The PL area was delimited based on Dcx expression. The "cell counter" plugin was used to manually count labeled cells. Data are represented as the sum of analyzed fields per section. We analyzed at P30, 2 animals, 7 sections, 33 images, and 1611 Dcx^+ cells; at P40, 2 animals, 4 sections, 16 images, and 446 Dcx^+ cells; and at P67: 3 animals, 6 sections, 20 images, and 921 Dcx^+ cells. Because the number of animals was insufficient to perform statistical analysis, we present descriptive statistics for the Tbr1 and CoupTFII quantifications—for Tbr1, at P30 (n = 33, range = 89.4, mean = 53.6, SD = 29.1), at P40 (n = 16, range = 88.4, mean = 52.0, SD = 27.0), and at P67 (n = 20, range = 100, mean = 31.3, SD = 30.3); for CoupTFII, at P30 (n = 33, range = 76.6, mean = 65.3, SD = 19.1), at P40 (n = 16, range = 42.4, mean = 73.5, SD = 11.7), and at P67 (n = 20, range = 100, mean = 41.6, SD = 36.5).

All graphs and relative statistical analysis were performed using GraphPad Prism (San Diego, California, USA).

3 | Results

3.1 | Adult Ferret PL and Comparison to Other Regions With Immature Neurons

We began by exploring whether the adult ferret (*M. putorius furo*), a small gyrencephalic mammal in the Mustelidae family, had immature neurons in the amygdala. We identified a large population of immature neurons and mapped the location of the region containing Dcx^+Psa-$Ncam^+$ cells in serial sections beginning at the anterior end of the amygdala and extending caudally to the hippocampus (Figure 1A). In the lateral and ventral amygdala, we found a region with Dcx^+ cells (8.6% of total Dcx^+ neurons, Figure 1B and Table 4) present in dense clusters (Figure 1B) as well as distributed fields of individual cells extending into the BLA and adjacent cortical regions. The spatial distribution of these cells resembles that of the PL in other mammalian species. We considered Dcx^+ cells with nuclei not closely associated with one another as "dispersed Dcx^+ cells" (Figure 1C). These "dispersed cells" were found distributed within adjacent subregions of the amygdala, consistent with the possibility that they were migrating into these neighboring regions. In addition to the "dispersed Dcx^+ cells" extending into the amygdala, we also observed "clustered Dcx^+ cells," which we defined as those Dcx^+ cells with nuclei tightly associated with one another in small collections (Figure 1D).

We next co-immunostained adjacent sections with Psa-Ncam (Figure 1E) and Sox11 (Figure 1F). The majority of dispersed (Figure 1Ei,Fi) or clustered Dcx^+ cells (Figure 1Eii,Fii) co-expressed Psa-Ncam and Sox11, suggesting they are in an immature state. Many of the individually dispersed Dcx^+ cells extending into the amygdala had a migratory neuron morphology, with an elongated nucleus and 1 or 2 Dcx^+ processes (Figure 1Fiii). These processes had a range of diverse orientations. Together, these results show that the ferret amygdala has a homologous region with immature neurons corresponding to the PL observed in other mammals.

To further investigate the immature and migratory features of these neurons, we studied their ultrastructure in adults. Within the PL region containing Dcx and Sox11 co-expressing cells (Figure 2A), we collected high magnification images using transmission electron microscopy. We observed dense collections of cells (see left side of overview in Figure 2B) compared to the lower overall cellular density in the rest of the amygdala. TEM overview images showed that these dense clusters of nuclei were located between the BLA and dense myelinated regions containing oligodendrocytes in the external capsule. Immature neurons appeared in clusters (left side of overview in Figure 2B), individually (middle of overview in Figure 2B), and in pairs (right side of overview in Figure 2B). They were identifiable by their ultrastructural features: Their nucleus was slightly irregular but did not contain deep invaginations and had many dense regions with heterochromatin closely associated with the nuclear membrane; they had very little cytoplasm, bringing the nuclear envelope into close proximity with the cell membrane. Within this limited cytoplasmic rim, we observed free ribosomes, short

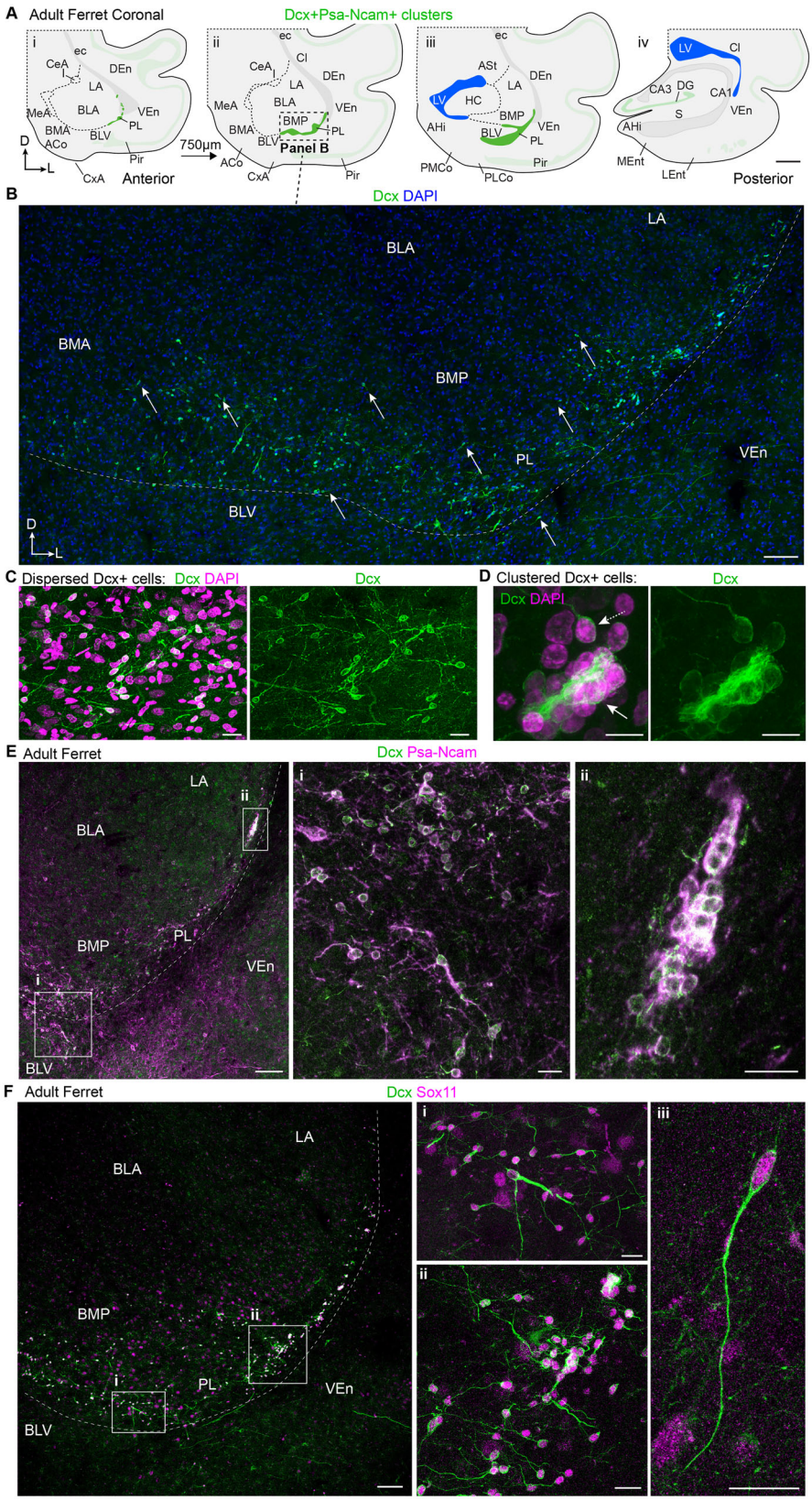

FIGURE 1 | Legend on next page.

endoplasmic reticulum cisternae, a small Golgi apparatus, and mitochondria; however, there were far fewer of these organelles than in mature neurons (Figure 2C,D).

We next examined the structures surrounding the immature PL neurons, which frequently included additional immature neurons and astrocytes, as well as the (primarily unmyelinated) axons present in this region. We also observed intercellular gaps—electron-lucent regions where the cell membranes do not touch—between PL cells and their surroundings. These gaps occurred between the immature neurons and surrounding structures, including other immature neurons, astrocytic processes, and dendrites. The intercellular gaps were small and punctuated by membrane extensions from the immature neurons (Figure 2Cii) or displayed a thin and continuous contour (Figure 2Ci). Astrocyte expansions frequently contacted immature neurons and were electron-lucent and contained intermediate filaments (Figure 2Ci,Di,Dii). Astrocytic processes extending between immature neurons were also bordered by intercellular gaps. The astrocytic expansions frequently enveloped both dispersed and clustered PL neurons, but they did not completely isolate them from the surrounding tissue (Figure 2Ci). These ultrastructural observations of immature neurons in the adult PL reveal contacts with surrounding cells that are consistent with their ability to migrate and/or grow in size and complexity with maturation.

To further investigate immature PL neuron contacts with their surroundings, we compared them to other regions known to contain immature neurons: the neurogenic dentate gyrus and the non-neurogenic piriform cortex. Compared to the PL, immunostaining of the adult ferret piriform cortex revealed small neurons with few processes and many larger, branched, Dcx^+Sox11^+ neurons (Figure 2E). The ultrastructure revealed a different environment surrounding the immature neurons in the piriform cortex (Figure 2F). Unlike the PL, most individual immature neurons in the piriform cortex were not in clusters but surrounded by astrocytes and mature neurons, axons, and dendrites, including synapses. The contacts with these neighboring cells included adherens junctions, typical of immature neurons. The intercellular gaps that surround immature neurons in the PL were rare in piriform cortex (Figure 2F); when present, these gaps were small in size (Figure 2H). Neighboring astrocyte expansions were variable, either not visible (Figure 2F), infrequent (Figure 2G), or abundant (Figure 2H). Intracellular features of piriform cortex immature neurons shared similarities to those in the PL, including slightly irregular or elongated nuclei. In the piriform cortex, these cells also had compacted chromatin and limited cytoplasm with few organelles; however, the cytoplasm was larger, and there was less compacted chromatin compared to the PL immature neurons. These observations suggest that the adult ferret piriform cortex contains immature neurons with ultrastructural features similar to those of PL (possibly more mature), but dispersed, with less ensheathing of astrocytic processes and more extensive contact with surrounding neurons.

Next, we examined immature neurons in the adult ferret hippocampus, a known site of adult neurogenesis and short-distance migration of new neurons into the granule cell layer. In this region, we observed many small Dcx^+Sox11^+ cells, some exhibiting migratory features (Figure 2I). The majority of these cells were located in the subgranular zone of the dentate gyrus, with larger cells displaying weaker immunolabeling found deeper into the granule cell layer. Ultrastructural analysis revealed numerous mature granule neurons adjacent to immature neurons in the subgranular zone (Figure 2J). These immature neurons were surrounded by intercellular gaps and formed adherens junctions with neighboring cells, consistent with actively migrating neurons (Figure 2J, arrow). They also shared the ultrastructural characteristics of immature neurons described above, like an irregular nucleus shape, compacted chromatin, limited cytoplasm, and few organelles. Interestingly, the compacted chromatin in the immature PL neurons was more prominent compared to the immature neurons in either the piriform cortex or hippocampus.

Together, the immature neurons across adult brain regions in the ferret share ultrastructural features. However, compared to piriform and dentate immature neurons, PL immature neurons were frequently found in clusters with more intercellular gaps, and these cells had more extensive ensheathment by astrocytic processes.

3.2 | Anatomical Localization and Molecular Markers of the Juvenile Ferret PL

To explore the formation of the PL in the ferret amygdala, we studied juvenile brains aged ~1 to 2 months (P40–P65; see Table 1). To delineate amygdala subnuclei, we prepared serial coronal brain sections at P65 and used Timm's staining, which labels $zinc^+$ glutamatergic synapses with high contrast (Mizukawa et al. 1989) (Figure 3A,B). The amygdala was

FIGURE 1 | **Immature neurons in the adult ferret amygdala**. (A) Schematic representation of four anterior to posterior coronal sections spaced by 750 μm from the adult ferret brain. The region we considered PL is indicated based on the presence of $Dcx^+Psa\text{-}Ncam^+$ cells (green). (B) Dcx immunofluorescence in a coronal section showing the PL extending as a thin band of Dcx^+ clusters between the VEn and the BMA in a distributed field of immunolabeled cells. A subpopulation has migratory morphology (arrows). (C and D) Ventrally they appear as individual cells (C), and dorsally, they appear in tight clusters (D). (E and F) The majority of PL Dcx^+ cells co-express Psa-Ncam (E) and Sox11. (F) Dcx^+Sox11^+ cells appear as individual cells (Fi) and clusters (Fii) and display migratory morphology (Fiii) (not shown in overview). Scale bars: 1 mm (A), 100 μm (B, E, F), 20 μm (C, Ei, Eii, Fi, Fii, Fiii), and 10 μm (D). A, anterior; ACo, cortical amygdala; AHi, amygdalohippocampal area; ASt, amygdalostriatal transition area; BLA, basolateral amygdala; BLV, ventral basolateral amygdala; BMA, basomedial amygdala; BMP, posterior basomedial nucleus; CA1, cornu ammonis 1; CA3, cornu ammonis 3; CeA, central amygdala; Cl, claustrum; CxA, amygdaloid cortex; D, dorsal; DEn, dorsal endopiriform cortex; DG, dentate gyrus; ec, external capsule; HC, hippocampus; I, intercalated nuclei; LA, lateral amygdala; LEnt, lateral entorhinal cortex; LV, lateral ventricle; MeA, medial amygdala; MEnt, medial entorhinal cortex; Pir, piriform cortex; PL, paralaminar nuclei; PLCo, posterolateral cortical nucleus of the amygdala; PMCo, posteromedial cortical nucleus of the amygdala; S, subiculum; VEn, ventral endopiriform cortex.

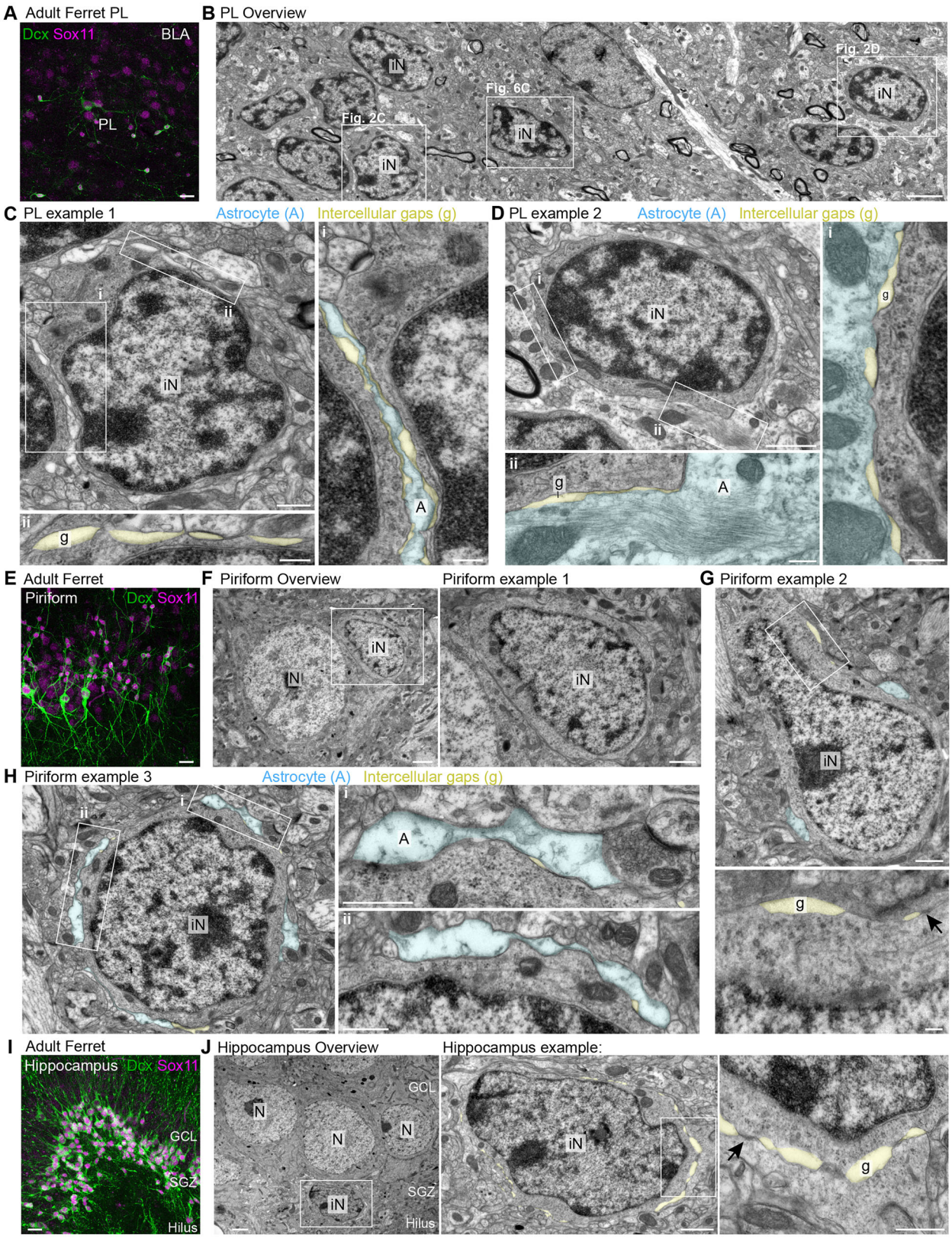

FIGURE 2 | Legend on next page.

present in four coronal sections spaced by 750 μm, with a ventral to dorsal gradient of staining visible within each of the subnuclei.

Next, we immunostained a series of adjacent sections for Dcx, GFAP, and NeuN, which highlighted a white matter boundary containing GFAP$^+$ fibers and cell bodies between the BLA and neighboring endopiriform regions (Figure 3C–F). There were small collections of Dcx$^+$ cells in this boundary separating the amygdala from the cortex (Figure 3D). Higher magnification images identified dense collections of Dcx$^+$ cells in clusters and fields of individual Dcx$^+$ cells extending into the neighboring amygdala nuclei (16.67% and 4.55% of total Dcx$^+$ cell population at P40 and P66, respectively, Figure 3E and Table 4).

To determine whether juvenile ferret PL neurons have a similar molecular identity to PL neurons in young humans and mice, we immunolabeled adjacent sections for CoupTFII, Ctip2, and Tbr1, transcription factors expressed by PL neurons in those species (Alderman et al. 2024). We examined sections from brains at postnatal days P30, P40, and P67, roughly corresponding to mouse postnatal days P14, P18, and P28, respectively (Figure S1). Coronal sections revealed many CoupTFII and Tbr1 immunopositive neurons in the BLA (Figure 4A,B). At these ages, the PL was visible lateral to the BLA as a field of Dcx$^+$ cells, which co-expressed Tbr1, CoupTFII, and Ctip2 but were negative for FoxP2 and Satb2 (Figure 4C). Approximately 60% of Dcx$^+$ cells co-expressed Tbr1 at P30, and this percentage decreased to ~30% by P67. Similarly, the proportion of Dcx$^+$CoupTFII$^+$ cells declined sharply after P40 to about half of that observed at P30 (Figure 4D).

At the juvenile ages studied (P30, P40, and P67), not all Dcx$^+$Tbr1$^+$ cells co-expressed CoupTFII. Some Dcx$^+$ cells were positive only for Tbr1, whereas others expressed only CoupTFII. The relative proportions of these two populations remained stable over time. However, the percentage of Dcx$^+$ cells co-expressing both Tbr1 and CoupTFII decreased with age, particularly after P40, whereas the proportion of Dcx$^+$ cells negative for both markers increased (Figure 4E,F). The dense clusters of cells in the PL have sometimes been grouped with the intercalated nuclei; however, unlike PL cells, the intercalated nuclei in the ferret brain exhibit little to no Dcx expression at juvenile ages, and were positive for FoxP2 (Figure 4G–J).

3.3 | Migratory Features of PL Neurons in Adult and Juvenile Ferret

Our observations of immature PL neurons in juvenile and adult ferrets suggested that a subpopulation of these neurons might have the ability to remodel their structure postnatally via continuing growth or migration. To investigate this possibility further, we compared the relationship between immature PL cells and their surroundings across ages (Figures 5 and 6). We began with a comparison of PL cell clusters as this configuration has been observed for migratory neurons in the adult ferret V-SVZ (Takamori et al. 2014).

In the adult ferret amygdala, we observed very thin astrocytic processes between clustered cells (Figure 5Bi) and abundant intercellular gaps (Figure 5Bii), features that are consistent with these cells moving or remaining flexible relative to their surroundings. At juvenile ages (P47 and P66), the PL cells in clusters were also surrounded by intercellular gaps and had adherens junctions between them (Figure 5C,D). At P66, we observed astrocytic expansions coming into direct contact with the immature neurons and limiting the amount of direct contact between immature neurons (Figure 5D). We also frequently observed transverse cross-sections of multiple bundled processes densely filled with microtubules (Figure 5C,D insets, Supporting Information Movie 1). These process bundles were surrounded by abundant free spaces and astrocyte extensions, hallmarks of migration. Immature neurons with these characteristics were confirmed as Dcx$^+$ by pre-embedding immunogold labeling (Figure 5E).

To quantitatively assess the surroundings of immature neurons in juveniles and adults, we measured the percentage of intercellular gaps, astrocytes, or other elements surrounding each immature soma (either in clusters or isolated) (Figure 5F–H). This analysis revealed that astrocyte contacts did not significantly change with age. The intercellular gaps decreased slightly between P47 and P66 and were still present in adults (15.03% ± 7.3 *SD*), consistent with the possibility of active migration or cellular rearrangement occurring at all ages. To further explore the presence of intercellular gaps in adults, we evaluated Dcx$^+$ clusters and found examples of process bundles that also appeared to emanate from multiple cells. Ultrastructural evaluation of these adult process bundles revealed that, similar to juveniles (Figure 5C,D), they had an irregular shape, an abundance of

FIGURE 2 | Ultrastructural comparison between regions with immature neurons in adult ferrets. (A) Double immunofluorescence of Dcx and Sox11 co-expression in PL neurons. (B) TEM overview of the PL showing immature neurons within a neuropil rich in unmyelinated axons and astrocytic processes. (C and D) Representative PL immature neurons have little cytoplasm, irregular nuclei with clumped chromatin, and frequent intercellular gaps (yellow). Astrocytic processes containing intermediate filaments (blue) partially surround the immature neurons. (E) Double immunofluorescence labeling of Dcx and Sox11 co-expression in layer 2/3 of the piriform cortex. (F) TEM overview of layer 2/3 of the piriform cortex showing an immature neuron adjacent to a mature neuron. (G and H) Immature neurons display irregular nuclei with compact chromatin and cytoplasm rich in free ribosomes but poor in organelles. Intercellular gaps (yellow) are infrequent, and astrocytic processes containing intermediate filaments (blue) surround the cells, which occasionally form adherens junctions (arrow). (I) Double immunofluorescence of Dcx and Sox11 co-expression in the DG. (J) TEM overview of the DG with an immature neuron located in the SGZ near mature granule neurons. Immature DG neurons have little cytoplasm, clumped chromatin, and irregular nuclei, with frequent intercellular gaps (yellow) and occasional adherens junction contacts (arrow). Scale bars: 20 μm (A, E, I), 2 μm (B, F, J), 1 μm (D, F (right) and J (middle), G, H), 500 nm (C, Hi, Hii, J (right)), and 200 nm (Ci, Cii, Di, Dii, G (bottom)). DG, dentate gyrus; GCL, granule cell layer; iN, immature neuron; N, mature neuron; SGZ, subgranular zone.

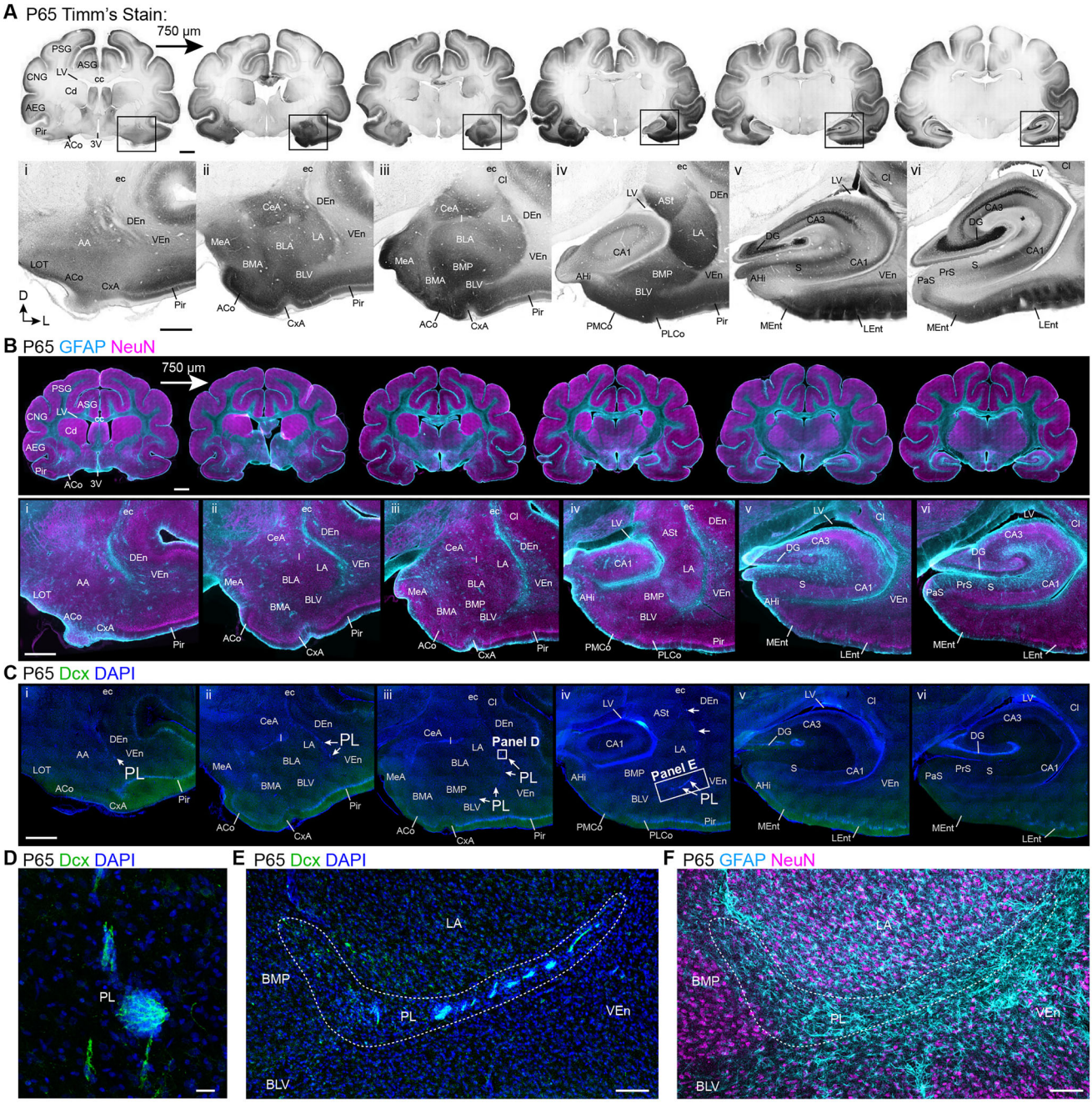

FIGURE 3 | **Anatomical location of the PL in juvenile ferrets**. (A) Timm's staining of a series of coronal sections from the juvenile (P65) ferret brain spaced by 750 µm showing the anatomical subregions of the juvenile ferret amygdala. (B) Immunofluorescence of GFAP and NeuN in serial coronal sections with anatomical labels based on staining in part (A). (C) Immunofluorescence for Dcx together with DAPI from the same sections in part (B). Arrows point to the PL and areas shown at higher magnification (D–F). (D) High magnification of Dcx^+ clusters in the dorsolateral PL. (E and F) High magnification of the Dcx^+ cells in the ventromedial PL (E). Dotted line indicates the same region in parts (E) and (F), which extends along the ventral amygdala from the VEn to the BMP. This region is rich in $GFAP^+$ cells and poor in NeuN expression (F). Scale bars: 2 mm (A, B top line), 1 mm (A, B bottom line, C), 100 µm (E, F), and 20 µm (D). AA, anterior amygdaloid area; ACo, cortical amygdala; AEG, agranular insular area; AHi, amygdalohippocampal area; ASG, anterior sigmoid gyrus; ASt, amygdalostriatal transition area; BLA, basolateral amygdala; BLV, ventral basolateral amygdala; BMA, basomedial amygdala; BMP, posterior basomedial nucleus; CA1, cornu ammonis 1; CA3, cornu ammonis 3; CeA, central amygdala; Cl, claustrum; CNG, coronal gyrus; CxA, amygdaloid cortex; D, dorsal; DEn, dorsal endopiriform cortex; DG, dentate gyrus; ec, external capsule; I, intercalated nuclei; LA, lateral amygdala; LEnt, lateral entorhinal cortex; lot, lateral olfactory tract; LV, lateral ventricle; MeA, medial amygdala; MEnt, medial entorhinal cortex; PaS, parasubiculum; Pir, piriform cortex; PL, paralaminar nuclei; PLCo, posterolateral cortical nucleus of the amygdala; PMCo, posteromedial cortical nucleus of the amygdala; PrS, presubiculum; PSG, posterior sigmoid gyrus; S, subiculum; VEn, ventral endopiriform cortex; 3V, third ventricle.

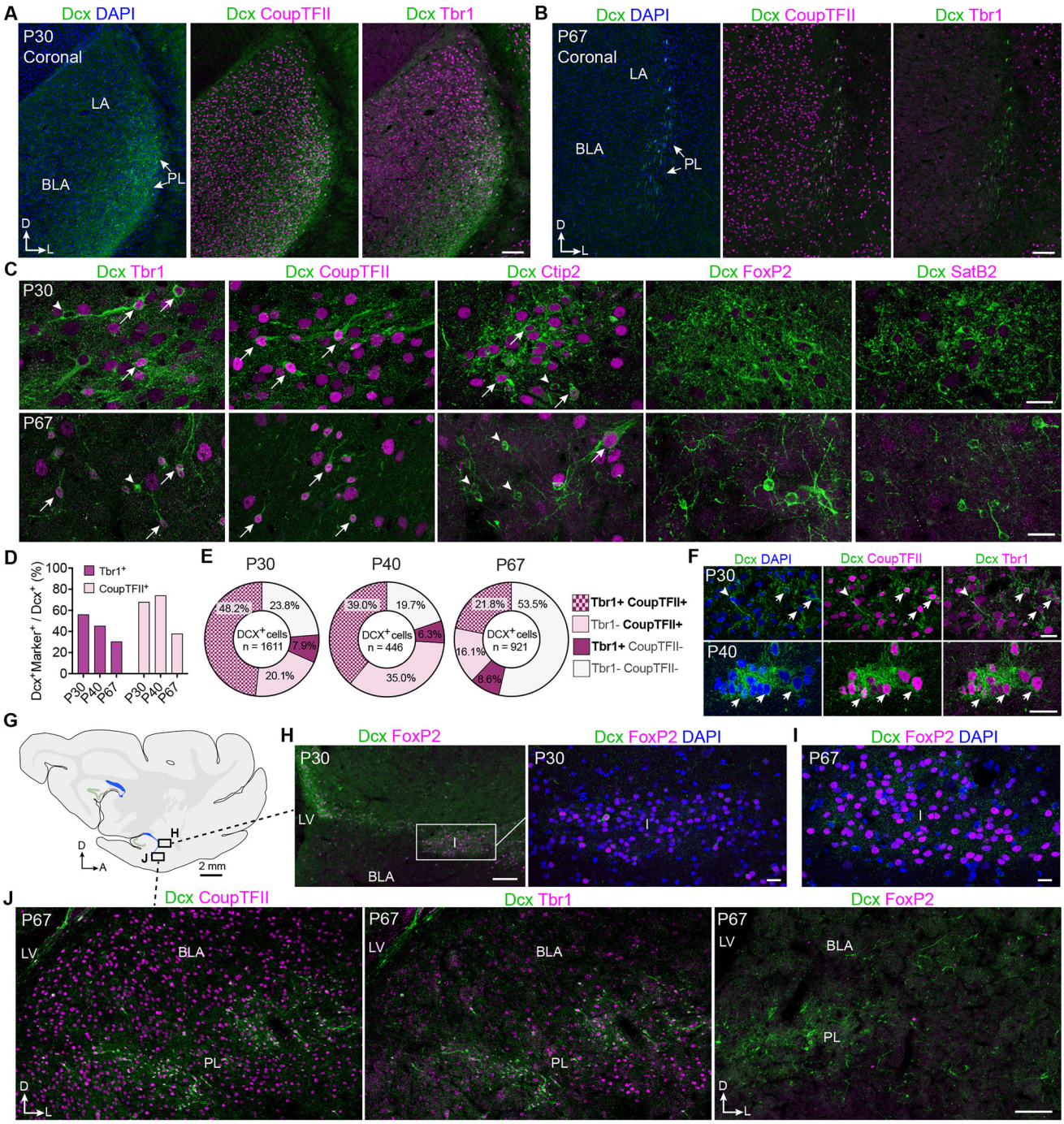

FIGURE 4 | **Molecular characterization of Dcx$^+$ cells in the juvenile ferret PL.** (A and B) Immunofluorescence for Dcx, CoupTFII, and Tbr1 in coronal ferret brain sections at P30 (A) and P67 (B). (C) Immunofluorescence for Dcx$^+$ cells in the PL at P30 and P67 showing co-localization (arrows) or absence of co-localization (arrowheads) with Tbr1, CoupTFII, or Ctip2. Dcx cells at both ages do not exhibit co-localization with FoxP2 or Satb2. (D) Quantification of the percentage of Dcx$^+$Tbr1$^+$ and Dcx$^+$CoupTFII$^+$ cells. (E) Pie charts showing the percentage of Dcx$^+$ cells positive for only one, both, or neither transcription factor at P30, P40, or P67. (F) Representative images of Dcx$^+$Tbr1$^+$CoupTFII$^+$ cells (arrows) and Dcx$^+$Tbr1$^-$CoupTFII$^-$ cells (arrowheads) at P30 and P40. (G) Schematic sagittal section of the ferret brain indicating the locations of the intercalated nuclei (I) and the PL. (H and I) Insets show FoxP2 expression in the intercalated nuclei (I), which are largely Dcx negative at these ages. (J) In the PL (bottom), many Dcx$^+$ cells are CoupTFII$^+$ and Tbr1$^+$, but FoxP2 negative. Scale bars: 100 μm (A, B, H, J) and 20 μm (C, F, H magnification, I). BLA, basolateral amygdala; D, dorsal; I, intercalated nuclei; L, lateral; PL, paralaminar nuclei.

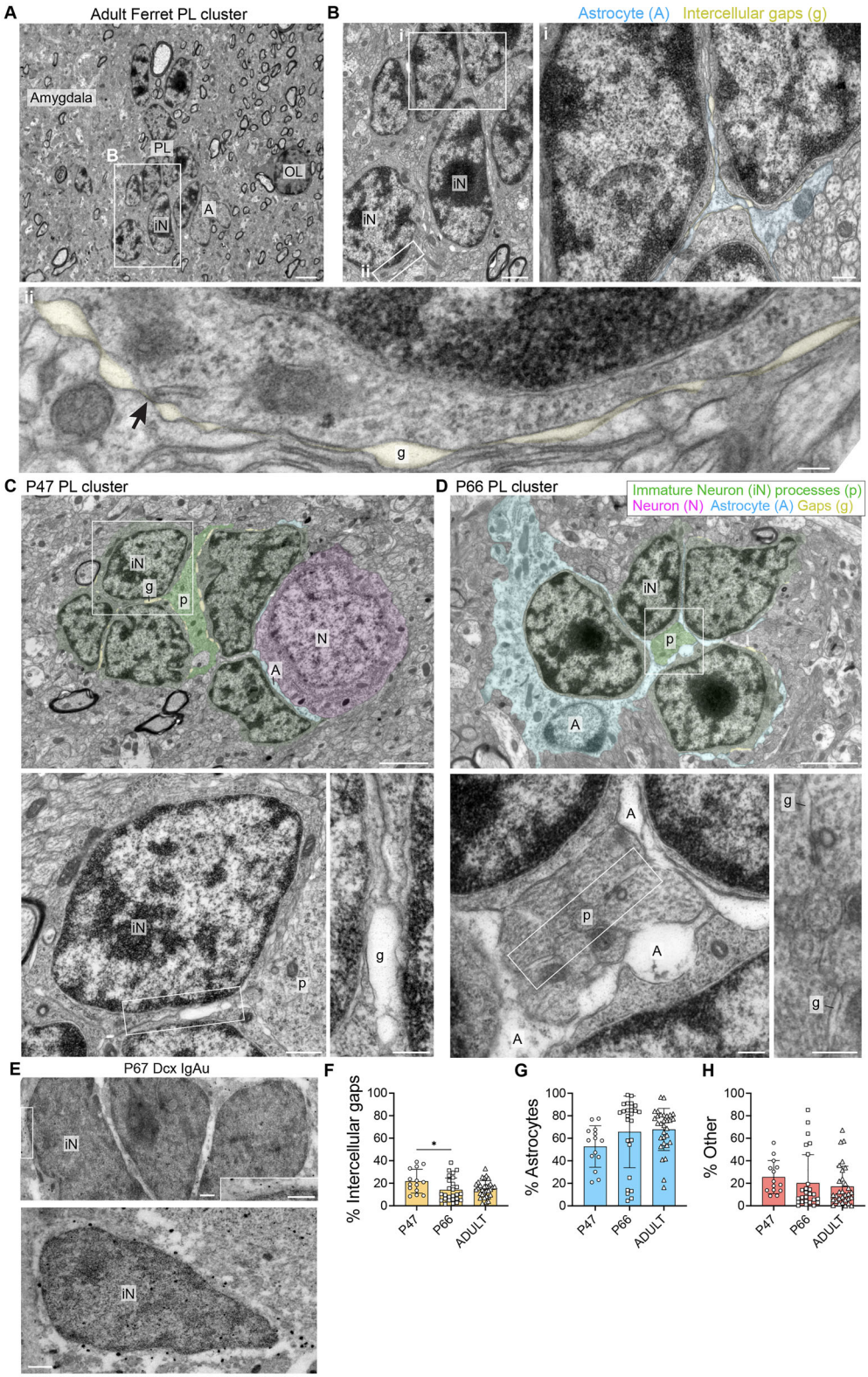

FIGURE 5 | Legend on next page.

intercellular gaps, and dense collections of transverse cross-sections of microtubules (Figure 6A,B). Although some of these features are also found in axons, axons are typically smaller, more rounded, have fewer spaces between them, and have fewer and more regular microtubules.

In adults, the isolated immature PL cells had ultrastructural features consistent with migration, including an elongated nucleus, scarce cytoplasm, and intercellular gaps (Figure 6C). To study these isolated Dcx^+ cells more comprehensively at each age, we used confocal microscopy to compare their soma elongation

index (SEI), or the ratio of the primary (long axis) to orthogonal axis (short axis) of the cell soma (Figure 6D–I). This analysis revealed a continuous distribution of elongation indices at all ages, ranging from ~0.5 to 1 (Figure 6G–I). Those Dcx$^+$ cells with an SEI near 0.5, or a primary axis roughly twice the length of the orthogonal axis, were the most elongated and frequently had a single process. Those Dcx$^+$ cells with SEI near 1 were nearly completely round and frequently had multiple, branched processes (Figure 6D–I). The cross-sectional area of the Dcx$^+$ cells with the most elongated features tended to be lower compared to the rounded cells, indicating that the elongated cells were generally smaller.

To further explore the relationship between Dcx$^+$ cell clusters and astrocyte (GFAP$^+$) processes, we used deconvolution confocal microscopy in juveniles (P40 and P66). We identified GFAP$^+$ astrocytes and their processes next to the clusters of Dcx$^+$ cells. At both ages, the GFAP$^+$ somas were located near the clusters of Dcx$^+$ cells, and their processes appeared to surround and extend into the clusters, similar to the astrocyte expansions detected within the clusters using TEM. These fibers had multiple contact points within the clusters and, in some instances, completely surrounded the soma of Dcx$^+$ neurons. At multiple points, the GFAP$^+$ processes branched, sometimes within the clusters. We further analyzed individual *z*-stacks of the deconvoluted confocal images, which confirmed these close appositions between GFAP$^+$ fibers and Dcx$^+$ cells (Figure 6J,K). Although our prior analysis found no significant change in overall astrocyte contacts with immature PL neurons across ages (Figure 5G), when we examined the astrocyte contacts with only those immature neurons in clusters, there was an increase in the percentage of direct astrocyte contacts (32.99% ± 11.91 *SD* at P47, to 67.28% ± 30.14 *SD* at P66, to 66.8% ± 19.59 *SD* in the adult), which correlated with a decrease in direct contacts between the immature cells in clusters (20.21% ± 4.91 *SD* at P47, to 1.67% ± 3.45 *SD* at P66, to 0% ± 0 *SD* in the adult). Together, these observations indicate that astrocytes separate immature neurons in clusters from each other and have extensive direct contacts with immature PL neurons in all ages.

3.4 | Cross-Species Comparison of PL Expansion Into the Amygdala

The PL is prominent in primates (including humans) relative to mice (Alderman et al. 2024; Sorrells et al. 2019; deCampo and Fudge 2012; Chareyron et al. 2011), but the connection between this increased association and evolutionary changes in brain size and complexity is unknown. Here, we compared the PL across mammals belonging to different orders and with different brain size and complexity. We selected sagittal sections from humans (15 years) and mice (P60), corresponding to late adolescent to early adult ages (Arellano et al. 2024; Figure 7A–F, Figure S1). Similar to previous descriptions in these species (Alderman et al. 2024; Sorrells et al. 2019), immunostaining for Dcx and Psa-Ncam revealed collections of immature neurons in both humans and mice. In mice, the immunolabeled cells were located primarily anterior to the BLA and did not extend into it (Figure 7A–C). In humans, dense clusters of Dcx$^+$Psa-Ncam$^+$ cells were present ventrally to the amygdala and extended dorsally into the basolateral nuclei (Figure 7D–F).

We next analyzed sagittal brain sections from a 3-year-old adult marmoset (*C. jacchus*) and found that the PL was similarly located to that in humans, forming a rostrocaudal continuum of Dcx$^+$Psa-Ncam$^+$ cells along the ventral boundary of the BLA (Figure 7G–I). This continuum can be subdivided into two regions: an anterior region composed of scattered individual cells and fiber bundles that gradually increase in density caudo-ventrally (region in Figure 7J–M from overview in Figure 7H) and a posterior region adjacent to the lateral ventricle that forms a large compact cellular cluster (region in Figure 7I from overview in Figure 7H). The Dcx$^+$ cells in these regions were also positive for Tbr1, indicating a glutamatergic (excitatory) neuronal identity (Figure 7M). However, most Dcx$^+$ cells did not express the mature neuron marker NeuN (Figure 7J,L), which could indicate that they are in a more immature state. These comparisons demonstrate that the PL association with the amygdala is independent of brain gyrification, as the lissencephalic marmoset has a much greater association with the amygdala compared to the lissencephalic mouse.

To compare PL cells in adult mouse, marmoset, ferret, and human, we quantified the densities of Dcx$^+$ and NeuN$^+$ cells and the percentage of the Dcx$^+$ population co-expressing NeuN. We found a conserved low percentage of Dcx$^+$ cells co-expressing NeuN across species, suggesting that most Dcx$^+$ cells in the region are in an immature state (Figure 7N–P). We did not detect significant density or co-localization percentage differences between species; however, these might be revealed by comparison of specific subregions or a larger sample size.

Together, these cross-species comparisons show that the increased association of the PL with the amygdala is found in primates with differing brain complexity and also in the ferret, a gyrencephalic mammal from a different order. The swine (*S. scrofa domesticus*) is a placental mammal within the same higher

FIGURE 5 | **Ultrastructural features of cell clusters in the ferret PL across ages.** (A) Overview TEM image showing a cluster of immature neurons located at the interface between the amygdala and heavily myelinated axon tracts. (B) The cluster is composed of tightly packed immature neurons. Astrocytic expansions (blue) extend into the cluster, partially isolating cells from one another (Bi). Intercellular gaps (yellow) are observed surrounding the immature neurons, as well as adherens junctions (arrow) between them (Bii). (C and D) TEM examples of clusters of immature neurons at P47 (C) and P66 (D). These clusters have frequent intercellular gaps (yellow) between the cells in the cluster and their surroundings that, in some cases, include more mature neurons. The clusters also are surrounded by and innervated by astrocytic expansions in between the immature neurons. In both cluster examples, there are dense collections of processes (p) converging from immature neurons that are filled with microtubules. (E) Pre-embedding immuno-gold for Dcx. Dcx$^+$ cells in a cluster (top) and an individual Dcx$^+$ cell (bottom). (F–H) Percentages of cell contour in contact with either intercellular gaps (F), astrocytes (G), or other structures (H). There is a significant decrease in the percentage of gaps between P47 and P66. ANOVA $p < 0.05$. Scale bars: 2 μm (A, C, D overview), 1 μm (B), 500 nm (C, bottom left, E), 200 μm (Bi, C bottom right, D bottom left), and 100 nm (Bii). A, astrocyte; g, intercellular gaps; iN, immature neuron; N, mature neuron; OL, oligodendrocyte; p, immature neuron processes; PL, paralaminar nuclei.

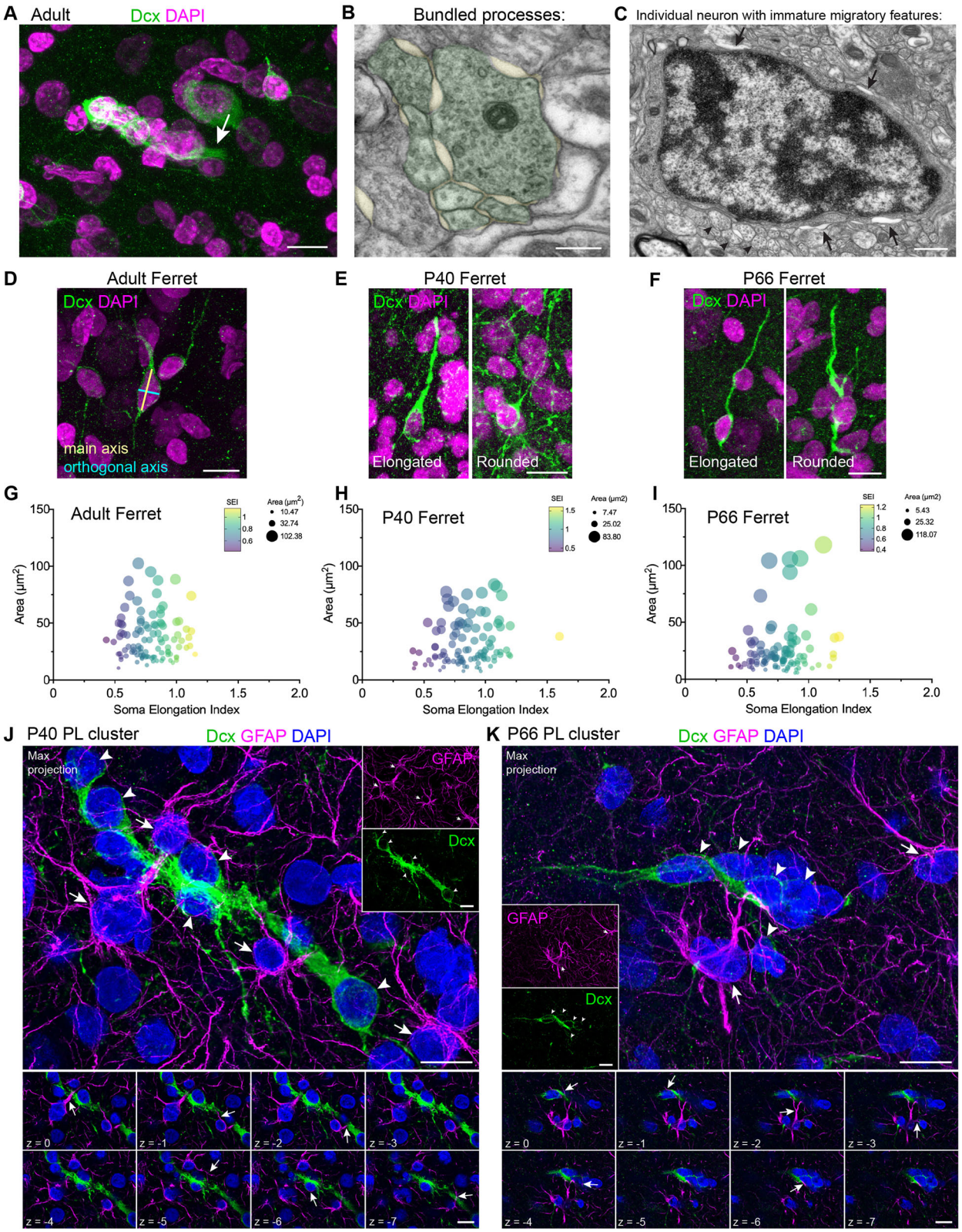

FIGURE 6 | Legend on next page.

order placental clade as the ferret (Laurasiatheria) but distinct from humans (Euarchontoglires). We compared the location of $Dcx^{+}Psa\text{-}Ncam^{+}$ cells across a series of sagittal sections from the juvenile (5-month-old) swine and the juvenile (P67) ferret (see Figure S1 for age comparisons). In the sagittal sections from juvenile (P67) ferrets, we observed densely packed clusters of $Dcx^{+}Psa\text{-}Ncam^{+}$ cells along the ventral BLA (Figure 8A–C), similar to what was observed in coronal sections in adults and juveniles (Figures 1 and 3). In the sagittal sections from the juvenile swine, the $Dcx^{+}Psa\text{-}Ncam^{+}$ cells were also located

at the ventral and rostral border of the BLA (Figure 8D,E), similar to ferrets and humans. Dcx$^+$Psa-Ncam$^+$ cells were found in large, compact clusters as well as cells arranged in thin chains (Figure 8F). The Dcx$^+$ cells from these regions were immunopositive for the excitatory neuronal markers CoupTFII and Tbr1 (Figure 8G,H), similar to ferret, mouse, marmoset, and human.

The above indicates that the PL region in the amygdala of the swine and the marmoset contains large collections of immature excitatory neurons (Dcx, Psa-Ncam, Tbr1, CoupTFII), similar to what is observed in humans and ferrets. Unlike the mice and similar to humans and ferrets, these putative immature neurons were more abundant, more widely distributed, and present as both clusters or dispersed cells in the swine and marmoset brains.

4 | Discussion

In this study, we describe the ferret PL in juveniles and adults and compare its cellular composition to other species with different gyrification indices and belonging to different orders. The ferret PL had homologous features to the PL in other mammalian species and contained an extensive collection of immature excitatory neurons, a subset of which had migratory morphology (elongated nuclei, intercellular spaces, limited cytoplasm, and a leading process). This was observed in both juveniles (P30, P40–44, P65–67) and adults (1.3 years). The immature PL neurons in ferrets extend into multiple amygdala nuclei, more closely resembling the dispersion of human PL compared to mice. This distribution in ferrets also resembles the immature neuron distribution in the amygdala of swine and marmosets, despite the large differences in phylogenetic relationships and brain complexity between these species. Together, these observations point to a similarity between the composition and organization of the PL and its increased association with the amygdala in ferrets, swine, marmosets, and humans, compared to rodents.

The anatomical location of the ferret PL at the ventro-lateral boundaries of the BLA is similar to humans (Sorrells et al. 2019), where it is primarily ventral to the BLA. In contrast, in mouse it sits more laterally and anteriorly to the BLA (Alderman et al. 2024). The dense clusters and dispersed Dcx$^+$Psa-Ncam$^+$ cells that we observed in ferrets are found in the PL of a range of other mammalian species, including mice (Alderman et al. 2024), rats (deCampo and Fudge 2012), non-human primates (Chareyron et al. 2016; Fudge 2004), and humans (Page et al. 2022; Sorrells et al. 2019). In both mice and ferrets, we also observed many Dcx$^+$Psa-Ncam$^+$ cells in the piriform cortex, similar to what has been reported in many species (Bonfanti et al. 1992; Luzzati et al. 2009; Xiong et al. 2008; Cai et al. 2009; Varea et al. 2011; Zhang et al. 2009; Gómez-Climent et al. 2008; Piumatti et al. 2018; La Rosa et al. 2020). PL-derived immature neurons mature into glutamatergic neurons in mice (Alderman et al. 2024), primates (Chareyron et al. 2012; Chareyron et al. 2016), and humans (Sorrells et al. 2019), based on their expression of excitatory markers. Consistently, many Dcx$^+$ cells in the juvenile ferret PL expressed Tbr1, Ctip2, and CoupTFII, but not FoxP2 or Satb2.

A subpopulation of ferret PL neurons displayed immature morphological and molecular characteristics, consistent with previous descriptions of immature PL neurons in mice (Alderman et al. 2024) and humans (Sorrells et al. 2019). A subset (15.8% of Dcx$^+$ cells SEI $\leq$0.5 from P40, P66, and adult PL) of isolated, immature PL neurons in ferrets had elongated morphology, small soma with a single leading process, expressed multiple markers of migratory neurons, and were surrounded by intercellular gaps, all of which are characteristics of migrating neurons (Doetsch et al. 1997; García-Verdugo et al. 1998). The targets of these migrating neurons have not been precisely determined; however, migration from the PL into the ventral endopiriform cortex is inferred in mice (Alderman et al. 2024). In humans (Sorrells et al. 2019) and other mammals (Ghibaudi et al. 2025), the cells with migratory morphology do not display a consistent orientation or directional migration into adjoining brain regions, suggesting they may complete their differentiation close to the PL region. Interestingly, in ferrets between P66 and adult ages, elongated Dcx$^+$ cells were frequently observed in the BLA. This is consistent with the possibility that ongoing migration from the PL into the BLA continues in the ferret. However, this apparent displacement of neurons could also be due to increasing neuropil as PL neurons mature. Although the molecular and morphological features of a subset of ferret PL neurons suggest active migration, this inference remains tentative. Future studies using live imaging or lineage tracing methods would be required to confirm active migration and the extent of neuronal displacement. We also do not know when these putative migrating cells in the ferret stop migrating and begin maturing. Verification of the trajectory of PL neuron maturation, migration, and final destinations will require more ages and additional technical approaches, such as viral lineage tracing or single-cell RNA-sequencing. We also do not know when immature PL neurons in the ferret and swine amygdala are born, but thymidine analog (e.g., BrdU) studies could identify the birthdate of these cells. Previous studies in sheep (Piumatti et al. 2018), which are laurasiatherian mammals

FIGURE 6 | **Migratory features of ferret PL neurons across ages**. (A) Immunofluorescence for Dcx showing a tight cluster of labeled nuclei and a single nearby cell. Clustered cells converge their processes into a common bundle (arrow). (B) TEM image of a tightly packed bundle of processes in this region (green) shows that they are microtubule-rich, irregular in shape, and are surrounded by many intercellular gaps (yellow). (C) TEM of an individual immature neuron with little cytoplasm, few organelles, clumped chromatin, and intercellular gaps (arrows). (D–F) Elongated and rounded Dcx$^+$ cells in adult (D), P40 (E), and P66 (F) ferret PL. For soma elongation index (SEI) analysis, the main axis (yellow) and orthogonal to main axis (cyan) were traced on the cell soma (D). (G–I) Bubble plot of Dcx$^+$ cell SEI and area analysis in adult (G), P40 (H), and P66 (I) ferret PL. SEI (*x*-axis, gradient color from purple to yellow indicates increasing SEI value) and cross-sectional area of each cell analyzed (*y*-axis, increasing size of the bubble indicates increasing area) are shown. (J and K) Immunofluorescence for Dcx (green) and GFAP (magenta) showing two different examples of immature clusters in the PL region at P40 and P66 (J and K top). Astrocytes (white arrows) are close to clusters of immature neuron somas (white arrowheads) (J and K bottom). Serial *z*-stacks confirming the apposition between GFAP$^+$ fibers and Dcx$^+$ cells. Sections were counterstained with DAPI (blue). Scale bars: 500 nm (C), 200 nm (B), 10 μm (A, D, E, F, J, K). PL, paralaminar nuclei; SEI, soma elongation index; TEM, transmission electron microscopy.

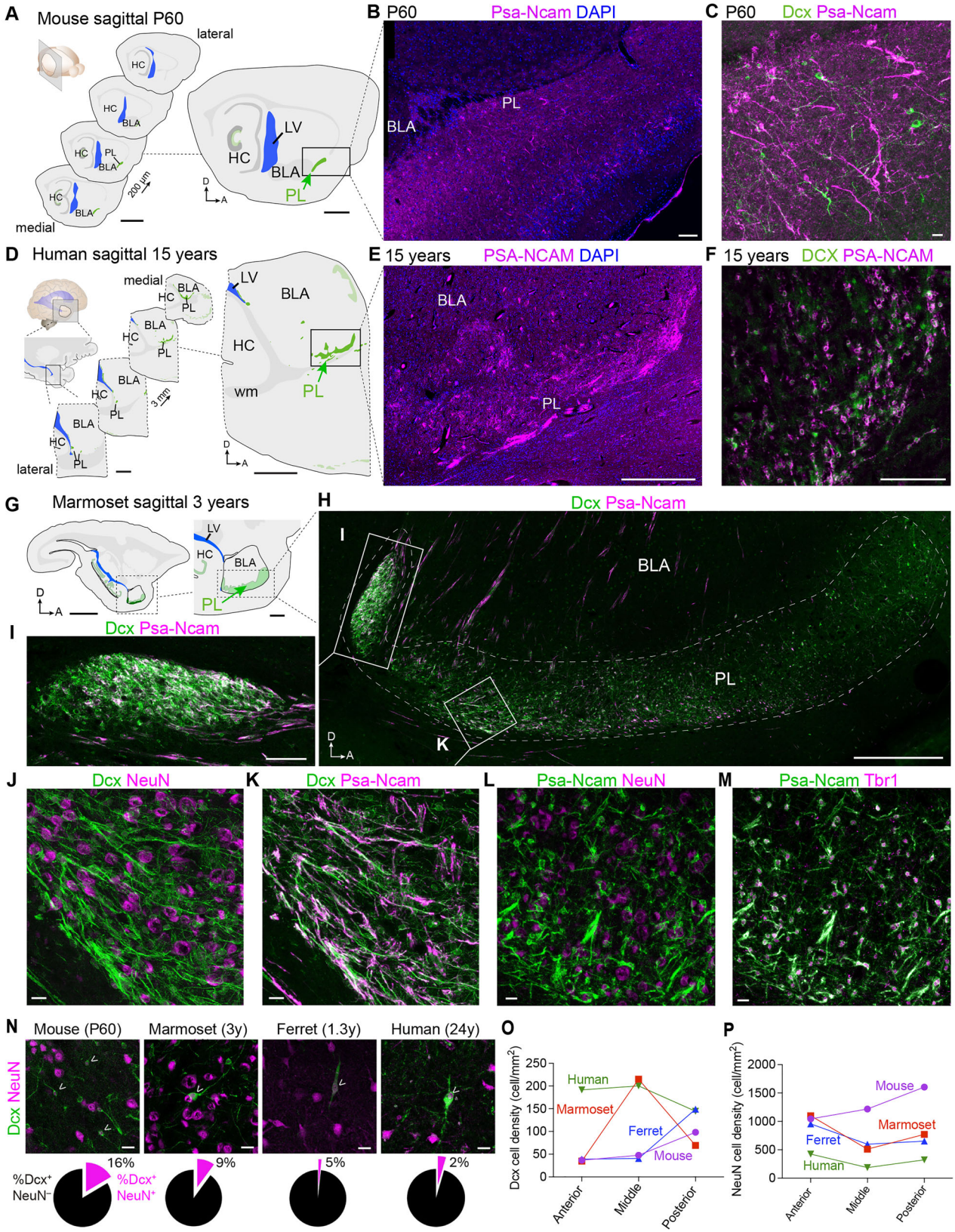

FIGURE 7 | Legend on next page.

like swine and ferrets, indicate that Dcx$^+$ cells in the adult amygdala are born during fetal development. This is similar to what has previously been observed in mice (Alderman et al. 2024) and suggests that these neurons may be born embryonically and remain immature for a prolonged time.

We also observed, in juvenile and adult ferrets, that many immature neurons in the PL form dense clusters, very similar to the clusters observed in the human PL (Page et al. 2022; Sorrells et al. 2019). Prior work evaluating migratory neurons in the ferret V-SVZ identified clusters of Dcx$^+$Psa-Ncam$^+$ cells (Takamori et al. 2014); however, PL clusters did not appear as a continuous migratory pathway. In some clusters, the collections of irregularly shaped fiber bundles with dense microtubules resembled migrating chains of neurons in the adult mouse V-SVZ (Doetsch et al. 1997). Ultrastructural and confocal microscopy analysis of these clusters revealed that they are partially surrounded by astrocytes and their processes; however, their association was reduced compared to the astrocyte ensheathment that occurs in the rostral migratory stream (Lois et al. 1996). We, therefore, do not believe that the ferret PL clusters correspond to chains of migrating young neurons but correspond to an accumulation of immature neurons. Whether these are reserve deposits of immature cells that then migrate outside of the clusters or mature locally remains unknown.

We identified differences in the surrounding cellular environment between the PL and other regions with immature neurons, such as the piriform cortex, which also contained many Dcx$^+$ neurons. Unlike the PL, immature neurons in the ferret piriform cortex were surrounded by astrocytes and few intercellular gaps. Similarly, astroglial lamellae and intercellular gaps have previously been found in close apposition to the plasma membrane of both Dcx$^+$ cell soma and processes in the adult mouse piriform cortex. This, together with the absence of synaptic contacts, could suggest that astrocytes have an insulating role, preventing Dcx$^+$ cells from receiving synaptic inputs (Gómez-Climent et al. 2008). Astrocytes promote proliferation, survival, and maturation of developing neurons and neuroblasts by secreting trophic factors and providing guidance cues for axons (Kandel 2013; Song et al. 2002). The association between Dcx$^+$ neurons and astrocytes could also suggest a supportive role of glia in the slow development of piriform cortex and PL neurons or the guidance to their final destination. However, we do not know whether immature neurons in ferrets are able to structurally and functionally integrate in the brain circuitry like in the mouse piriform cortex (Gómez-Climent et al. 2008; Rotheneichner et al. 2018; Benedetti et al. 2020). In ferrets, we also observed cells with migratory features in the PL but not in the piriform cortex, similarly to what has been previously reported in mice (Alderman et al. 2024; Klempin et al. 2011). The different cellular environments surrounding immature neurons in the PL or piriform cortex could result in a different impact on these neurons. Future studies identifying ligand-receptor pairs and signaling pathways from single-nuclei RNA-sequencing or spatial transcriptomics could potentially reveal whether there is a dynamic cross-talk between immature neurons and the surrounding cellular environment.

Comparative findings indicate that the presence of immature neurons in the amygdala is not exclusively linked to brain features like size or gyrencephaly. Immature neurons have been reported in the amygdala in mammals with a wide range of these brain features, including rodents (Nacher et al. 2002; Shapiro et al. 2009; Alderman et al. 2024), rabbits (Luzzati et al. 2003), voles (Fowler et al. 2003; Fowler et al. 2005), non-human primates (Bernier et al. 2002; Marlatt et al. 2011; Zhang et al. 2009), chimpanzees (Ghibaudi et al. 2025), and humans (Martí-Mengual et al. 2013; Sorrells et al. 2019; Li et al. 2023). The common marmoset is a primate with a lissencephalic brain, belonging to the same placental clade as humans, and the swine is an artiodactyl with a gyrencephalic brain, which belongs to Laurasiatheria like ferrets, and all three species have PL neurons extending into the BLA. Our results therefore show that species' evolutionary clade distance does not predict their increased prominence within the BLA. This agrees with a recent quantitative, comparative analysis of immature neurons in the amygdala, which found that the occurrence of immature neurons in the amygdala goes beyond the PL, extending into the BLA in gyrencephalic species and primates, and they are remarkably abundant in primates compared to other mammals (Ghibaudi et al. 2025). Compared to mice, the primate basolateral complex has also increased volume relative to the cortical and centromedial complexes, in conjunction with the expansion of the cerebral cortex (Chareyron et al. 2011; Chin et al. 2023; Ghibaudi et al. 2025). The presence of immature neurons has also been described in the cerebral cortex of widely different mammals (Gómez-Climent et al. 2008; Coviello et al. 2022; Piumatti et al. 2018; Li et al. 2023; Zhang et al. 2009; Cai et al. 2009; Luzzati et al. 2009; Pattaro et al. 2025), a population that is similarly expanded in large-brained species compared to small lissencephalic mammals (La Rosa et al. 2020). This phylogenetic trend may result from an evolutionary trade-off in plasticity, favoring different forms across species and brain regions in response to ecological pressures and functional demands (Bonfanti et al. 2024).

FIGURE 7 | **Comparison of PL relationship to the amygdala across species**. (A, D, G) Schematic representation of brain sagittal sections from mouse (A), human (D), and marmoset (G) PL, where green indicates regions with clusters of Dcx$^+$ and PSA-NCAM$^+$ cells. The location of the PL is indicated relative to the BLA for each species (green arrow). (B, E, H) Clusters of PSA-NCAM$^+$ cells labeled with immunofluorescence in the PL region in mouse (B), human (E), and together with Dcx in the marmoset (H). (C, F, I) Immunofluorescent labeling from the PL showing PSA-NCAM$^+$ cells also co-expressing Dcx in the studied species. (J–M) In the adult, 3 year old, marmoset, Psa-Ncam co-localizes with Tbr1, supporting an excitatory neuronal identity, whereas NeuN is predominantly expressed in Psa-NCAM$^-$ cells. (N) Top, Dcx$^+$NeuN$^+$ cells in adult mouse, marmoset, ferret, and human PL. Bottom: pie charts of Dcx$^+$NeuN$^+$ cells (purple) analysis over the total Dcx$^+$ cell population (black). (O) Linear plot of Dcx$^+$ cell density (cell/mm^2) and (P) NeuN$^+$ cell density (cell/mm^2) in adult mouse (purple), marmoset (orange), ferret (blue), and human (green) PL at each anatomical level considered for the analysis. Scale bars: 5 mm (A map series), 4 mm (G), 2 mm (D map series), 1 mm (A and D magnification, H), 100 μm (B, E, I), and 20 μm (C, F, J, K, L, M, N). A, anterior; Amyg, amygdala; BA, basal amygdala; D, dorsal; HC, hippocampus; LA, lateral amygdala; LV, lateral ventricle; PL, paralaminar nuclei; wm, white matter.

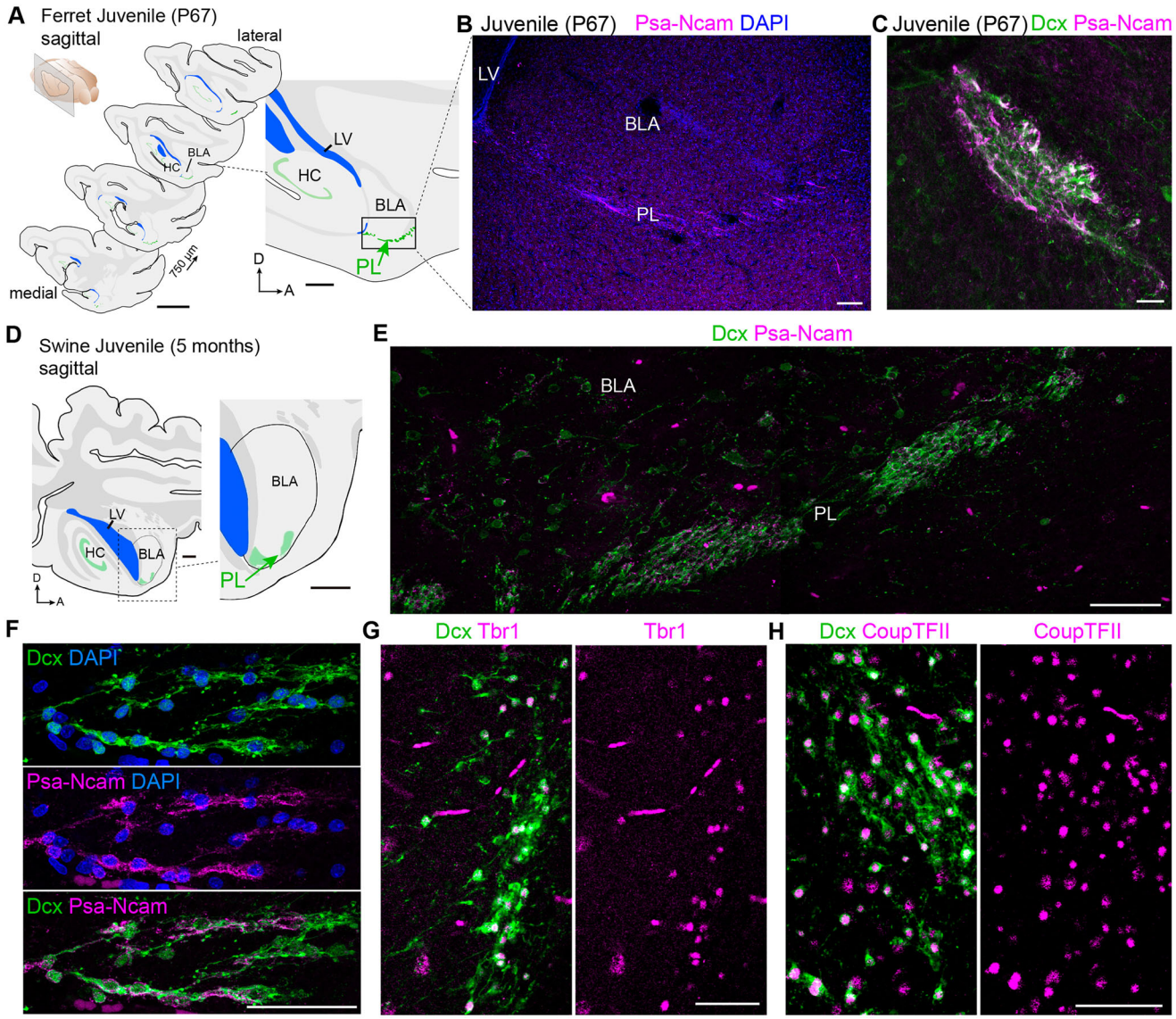

FIGURE 8 | **Comparison of juvenile PL in the gyrencephalic ferret and swine brains**. (A) Schematic representation of a sagittal section from the juvenile (P67) ferret with the PL indicated in green. (B) Immunofluorescence for Dcx and Psa-Ncam reveals the characteristic PL organization: A large and compact cluster is located caudally, whereas cells appear more scattered towards the ventrorostral pole. (C) Higher magnification image showing co-localization of Dcx and Psa-Ncam. (D) Schematic representation of a sagittal section of the juvenile (5-month-old) swine brain. The PL is highlighted in green. (E) Immunofluorescence for Dcx and Psa-Ncam. (F) High-magnification images where Psa-Ncam co-localizes with Dcx expression in cell clusters. (G and H) Immunostaining in coronal sections shows that Dcx^{+} cells in the swine PL co-expressed Tbr1 (G) and CoupTFII (H). Scale bars: 5 mm (A, D), 1 mm (A: inset), 500 µm (E), 100 µm (B), 50 µm (F, G, H), 20 µm (C). BLA, basolateral amygdala; Hip, hippocampus; LV, lateral ventricle; PirCx, piriform cortex; PL, paralaminar nuclei.

Although the functional significance of immature PL neurons in the amygdala remains unknown, studies in model systems offer a few clues for further investigation. Prior work in the marmoset has focused on the amygdala's synaptic mechanisms and network dynamics supporting emotional learning, stress regulation, and social behavior. Knockdown experiments of the endocannabinoid system in the marmoset amygdala have shown changes in anxiety and social behaviors (Zhu et al. 2023). Direct infusion of selective serotonin reuptake inhibitors into the marmoset amygdala has also been found to reduce anxiety-like behaviors (Quah et al. 2020). The amygdala connects to the prefrontal and anterior cingulate cortex (ACC) to form a network that drives a range of social behaviors, such as foraging, predator avoidance, and social communication (Murray and Fellows 2022). Alterations in the activity in these circuits are linked to behavioral abnormalities (Alexander et al. 2020). The delayed maturation of PL neurons is likely linked to modifications or maturation of these circuits. Studies discerning the quantification of factors influencing signaling and connectivity within PL-associated circuits will be necessary to understand the functional significance of this form of plasticity.

It has been proposed that plasticity in brain areas associated with social interaction, like the amygdala, could be connected to a species' degree of vocal learning and cooperative breeding (Biazzi et al. 2025; Sawiak et al. 2018). Similar to humans, marmosets

engage in socially guided vocal learning in early infancy and live in familial groups. Production of adult vocalizations nears proficiency around 6 months of age, with fine-tuning continuing into adulthood (Schultz-Darken et al. 2016). The many types of marmoset vocalizations have different behavioral meanings but can also serve as a coping strategy for emotional regulation (Cross and Rogers 2006). The marmoset amygdala contains neurons that can distinguish between vocalization types and caller identities, indicating its role in auditory perceptual processing (Jia et al. 2023). Thus, this prolonged PL plasticity could point to a phase of vocal learning in which adult marmosets learn to interpret infant vocalizations while helping raise their siblings and their own offspring around 3 years of age, in addition to emotionally regulating themselves and the group. It would be interesting to further investigate how the primate PL changes anatomically and functionally as sexual maturity is reached, and how these changes relate to cooperative breeding and offspring success.

Our study identifies the PL region in the ferret amygdala in juveniles and adults, and the migratory features of a subpopulation of the immature neurons found in this region. Comparison of the expansion of immature PL neurons into the amygdala across species revealed that its increased prominence is a shared trait in different mammals with a range of brain gyrification indices and phylogenetic lineages. Together, these observations provide a new comparative evolutionary look at postnatal amygdala development and can further facilitate the translation of results coming from different animal models.

5 | Conclusion

This study reveals structural, molecular, developmental, and evolutionary relationships of the PL region of the amygdala in mammals. Although the ferret belongs to a different evolutionary clade from humans and mice, the ferret PL has features that resemble those of each species. These include the presence of immature excitatory neurons expressing markers such as Dcx, Psa-Ncam, and Tbr1, and a subset of them with migratory characteristics in early postnatal stages and into adulthood. Similar to humans, ferret PL immature neurons extend into the rest of the BLA more than in mice, something we also observed in marmoset and swine. Together, these findings indicate that PL size and expansion into the rest of the amygdala occurs independently of brain size and cortical folding and suggest that the evolutionary rise of this form of plasticity across brain regions could instead relate to its functional significance.

Author Contributions

Lucía Inés Torrijos-Saiz, Shawn Sorrells, José Manuel García-Verdugo, and Vicente Herranz-Pérez conceived and designed the study. Lucía Inés Torrijos-Saiz designed and conducted experiments; analyzed data; and, together with Shawn Sorrells and Vicente Herranz-Pérez, wrote the first draft of the manuscript with input from all authors. Malaz Sharief and Marco Ghibaudi performed immunostaining and assisted in data interpretation, manuscript writing, and revisions. Lovisa Ljungqvist Brinson provided marmoset samples and manuscript edits and revisions. Funding and project supervision were provided by Shawn Sorrells and Vicente Herranz-Pérez. All authors reviewed and approved the final manuscript.

Acknowledgments

Lucía Inés Torrijos-Saiz has a predoctoral contract by the Valencian Council for Education, Universities, and Employment (ACIF2021/420). This work was supported by the Valencian Council for Education, Culture, University, and Employment (CIPROM/2023/053) to José Manuel García-Verdugo and Vicente Herranz-Pérez. The authors would also like to acknowledge the contributions of José Rodas Rodríguez who performed pilot immunostaining for this project. We thank Drs. David Rowitch and Justin Ellis for ferret tissue samples and early discussions of the project. We thank Loreta Medina and Ester Desfilis (Universitat de Lleida) for kindly providing the swine brain tissue used in this study. We thank Afonso C. Silva for kindly providing the marmoset brain tissue used in this study, with animal perfused by Seung Kwon Ha (DMV). Support was provided by NIH grants R01MH128745 and T32DC011499. Dr. Silva is funded by the National Institute on Aging (grants U19AG074866 and R24AG073190). Work in the Alvarez-Buylla laboratory is supported by NIH grants P01NS083513, R01NS028478, R35NS143000, and a generous gift from the John G. Bowes Research Fund. Arturo Alvarez-Buylla is the Heather and Melanie Muss Endowed Chair and Professor of Neurological Surgery at UCSF. Arturo Alvarez-Buylla is co-founder and on the Scientific Advisory Board of Neurona Therapeutics. This work is dedicated to the memory of Prof. José Manuel García-Verdugo, who sadly passed away during the completion of this article, leaving a lasting legacy in our lives and in science.

Ethics Statement

We declare that we adhere to the ethical and integrity policies of the journal regarding research. All protocols used were approved by institutional review committees as detailed in the methods.

Conflicts of Interest

The authors declare no conflicts of interest.

Data Availability Statement

The data supporting the findings of this study are available from the corresponding authors upon reasonable request.

References

Aerts, T., and E. Seuntjens. 2021. "Novel Perspectives on the Development of the Amygdala in Rodents." *Frontiers in Neuroanatomy* 15, no. December: 786679.

Ai, J.-Q., R. Luo, T. Tu, et al. 2021. "Doublecortin-Expressing Neurons in Chinese Tree Shrew Forebrain Exhibit Mixed Rodent and Primate-Like Topographic Characteristics." *Frontiers in Neuroanatomy* 15, no. September: 727883.

Alderman, P. J., D. Saxon, L. I. Torrijos-Saiz, et al. 2024. "Delayed Maturation and Migration of Excitatory Neurons in the Juvenile Mouse Paralaminar Amygdala." *Neuron* 112, no. 4: 574–592.e10.

Alexander, L., C. M. Wood, P. L. R. Gaskin, et al. 2020. "Over-Activation of Primate Subgenual Cingulate Cortex Enhances the Cardiovascular, Behavioral and Neural Responses to Threat." *Nature Communications* 11, no. 1: 5386.

Amaral, D. G., and J. L. Price. 1984. "Amygdalo-Cortical Projections in the Monkey (*Macaca fascicularis*)." *Journal of Comparative Neurology* 230, no. 4: 465–496.

Avino, T. A., N. Barger, M. V. Vargas, et al. 2018. "Neuron Numbers Increase in The Human Amygdala From Birth to Adulthood, But Not in Autism." *Proceedings of the National Academy of Sciences* 115, no. 14: 3710–3715.

Morais, A. G., P. Leonardo, M. García-Amado, et al. 2019. "Cyto- and Myelo-Architecture of the Amygdaloid Complex of the Common Marmoset Monkey (*Callithrix jacchus*)." *Frontiers in Neuroanatomy* 13, no. March: 441241.

Arellano, J. I., A. Duque, and P. Rakic. 2024. "A Coming-of-Age Story: Adult Neurogenesis or Adolescent Neurogenesis in Rodents?" *Frontiers in Neuroscience* 18, no. March: 1383728.

Barnette, A. R., J. J. Neil, C. D. Kroenke, et al. 2009. "Characterization of Brain Development in the Ferret via MRI." *Pediatric Research* 66, no. 1: 80–84.

Benedetti, B., D. Dannehl, R. König, et al. 2020. "Functional Integration of Neuronal Precursors in the Adult Murine Piriform Cortex." *Cerebral Cortex (New York, NY: 1991)* 30, no. 3: 1499–1515.

Bernier, P. J., A. Bédard, J. Vinet, M. Lévesque, and A. Parent. 2002. "Newly Generated Neurons in the Amygdala and Adjoining Cortex of Adult Primates." *Proceedings of the National Academy of Sciences of the United States of America* 99, no. 17: 11464–11469.

Biazzi, R. B., D. Y. Takahashi, and A. A. Ghazanfar. 2025. "Altricial Brains and the Evolution of Infant Vocal Learning." *Proceedings of the National Academy of Sciences of the United States of America* 122, no. 34: e2421095122.

Bonfanti, L., S. Olive, D. A. Poulain, and D. T. Theodosis. 1992. "Mapping of the Distribution of Polysialylated Neural Cell Adhesion Molecule Throughout the Central Nervous System of the Adult Rat: An Immunohistochemical Study." *Neuroscience* 49, no. 2: 419–436.

Bonfanti, L., C. La Rosa, M. Ghibaudi, and C. C. Sherwood. 2024. "Adult Neurogenesis and 'Immature' Neurons in Mammals: An Evolutionary Trade-Off in Plasticity?" *Brain Structure & Function* 229, no. 8: 1775–1793.

Bonfanti, L., and D. T. Theodosis. 2009. "Polysialic Acid and Activity-Dependent Synapse Remodeling." *Cell Adhesion & Migration* 3, no. 1: 43–50.

Brown, J. P., S. Couillard-Després, C. M. Cooper-Kuhn, J. Winkler, L. Aigner, and H. G. Kuhn. 2003. "Transient Expression of Doublecortin During Adult Neurogenesis." *Journal of Comparative Neurology* 467, no. 1: 1–10.

Cai, Y., K. Xiong, Y. Chu, et al. 2009. "Doublecortin Expression in Adult Cat and Primate Cerebral Cortex Relates to Immature Neurons That Develop Into GABAergic Subgroups." *Experimental Neurology* 216, no. 2: 342–356.

Chareyron, L. J., D. G. Amaral, and P. Lavenex. 2016. "Selective Lesion of the Hippocampus Increases the Differentiation of Immature Neurons in the Monkey Amygdala." *Proceedings of the National Academy of Sciences of the United States of America* 113, no. 50: 14420–14425.

Chareyron, L. J., P. Banta Lavenex, D. G. Amaral, and P. Lavenex. 2011. "Stereological Analysis of the Rat and Monkey Amygdala." *Journal of Comparative Neurology* 519, no. 16: 3218–3239.

Chareyron, L. J., P. Banta Lavenex, D. G. Amaral, and P. Lavenex. 2021. "Life and Death of Immature Neurons in the Juvenile and Adult Primate Amygdala." *International Journal of Molecular Sciences* 22, no. 13: 6691.

Chareyron, L. J., P. B. Lavenex, D. G. Amaral, and P. Lavenex. 2012. "Postnatal Development of the Amygdala: A Stereological Study in Macaque Monkeys." *Journal of Comparative Neurology* 520, no. 9: 1965–1984.

Chawana, R., N. Patzke, A. N. Alagaili, et al. 2016. "The Distribution of Ki-67 and Doublecortin Immunopositive Cells in the Brains of Three Microchiropteran Species, *Hipposideros fuliginosus*, *Triaenops persicus*, and *Asellia tridens*." *Anatomical Record (Hoboken, NJ: 2007)* 299, no. 11: 1548–1560.

Chin, R., S. W. C. Chang, and A. J. Holmes. 2023. "Beyond Cortex: The Evolution of the Human Brain." *Psychological Review* 130, no. 2: 285–307.

Conrad, M. S., R. N. Dilger, and R. W. Johnson. 2012. "Brain Growth of the Domestic Pig (*Sus scrofa*) From 2 to 24 Weeks of Age: A Longitudinal MRI Study." *Developmental Neuroscience* 34, no. 4: 291–298.

Coviello, S., Y. Gramuntell, P. Klimczak, et al. 2022. "Phenotype and Distribution of Immature Neurons in the Human Cerebral Cortex Layer II." *Frontiers in Neuroanatomy* 16, no. April: 851432.

Crosby, E. C., and T. Humphrey. 1941. "Studies of the Vertebrate Telencephalon. II. The Nuclear Pattern of the Anterior Olfactory Nucleus, Tuberculum Olfactorium and the Amygdaloid Complex in Adult Man." *Journal of Comparative Neurology* 74, no. 2: 309–352.

Cross, N., and L. J. Rogers. 2006. "Mobbing Vocalizations as a Coping Response in the Common Marmoset." *Hormones and Behavior* 49, no. 2: 237–245.

de Campo, D. M., and J. L. Fudge. 2012. "Where and What Is the Paralaminar Nucleus? A Review on a Unique and Frequently Overlooked Area of the Primate Amygdala." *Neuroscience and Biobehavioral Reviews* 36, no. 1: 520–535.

De Magalhães, J. P., and J. Costa. 2009. "A Database of Vertebrate Longevity Records and Their Relation to Other Life-History Traits." *Journal of Evolutionary Biology* 22, no. 8: 1770–1774.

Doetsch, F., J. M. Garcıá-Verdugo, and A. Alvarez-Buylla. 1997. "Cellular Composition and Three-Dimensional Organization of the Subventricular Germinal Zone in the Adult Mammalian Brain." *Journal of Neuroscience: The Official Journal of the Society for Neuroscience* 17, no. 13: 5046–5061.

Ellis, J. K., S. F. Sorrells, S. Mikhailova, et al. 2019. "Ferret Brain Possesses Young Interneuron Collections Equivalent to Human Postnatal Migratory Streams." *Journal of Comparative Neurology* 527, no. 17: 2843–2859.

Fasemore, T. M., N. Patzke, C. Kaswera-Kyamakya, E. Gilissen, P. R. Manger, and A. O. Ihunwo. 2018. "The Distribution of Ki-67 and Doublecortin-Immunopositive Cells in the Brains of Three Strepsirrhine Primates: *Galago demidoff*, *Perodicticus potto*, and *Lemur catta*." *Neuroscience* 372, no. February: 46–57.

Flügge, G., O. Ahrens, and E. Fuchs. 1994. "Monoamine Receptors in the Amygdaloid Complex of the Tree Shrew (*Tupaia belangeri*)." *Journal of Comparative Neurology* 343, no. 4: 597–608.

Fowler, C. D., M. E. Freeman, and Z. Wang. 2003. "Newly Proliferated Cells in the Adult Male Amygdala Are Affected by Gonadal Steroid Hormones." *Journal of Neurobiology* 57, no. 3: 257–269.

Fowler, C. D., F. Johnson, and Z. Wang. 2005. "Estrogen Regulation of Cell Proliferation and Distribution of Estrogen Receptor-Alpha in the Brains of Adult Female Prairie and Meadow Voles." *Journal of Comparative Neurology* 489, no. 2: 166–179.

Fudge, J. L. 2004. "Bcl-2 Immunoreactive Neurons Are Differentially Distributed in Subregions of the Amygdala and Hippocampus of the Adult Macaque." *Neuroscience* 127, no. 2: 539–556.

García-Verdugo, J. M., F. Doetsch, H. Wichterle, D. A. Lim, and A. Alvarez-Buylla. 1998. "Architecture and Cell Types of the Adult Subventricular Zone: In Search of the Stem Cells." *Journal of Neurobiology* 36, no. 2: 234–248.

Ghibaudi, M., C. La Rosa, N. Telitsyn, et al. 2025. "Multispecies Characterization of Immature Neurons in the Mammalian Amygdala Reveals Their Expansion in Primates." *PLoS Biology* 23, no. 8: e3003322.

Gleeson, J. G., P. T. Lin, L. A. Flanagan, and C. A. Walsh. 1999. "Doublecortin Is a Microtubule-Associated Protein and Is Expressed Widely by Migrating Neurons." *Neuron* 23, no. 2: 257–271.

Gómez-Climent, M. Á., E. Castillo-Gómez, E. Varea, et al. 2008. "A Population of Prenatally Generated Cells in the Rat Paleocortex Maintains an Immature Neuronal Phenotype Into Adulthood." *Cerebral Cortex (New York, NY: 1991)* 18, no. 10: 2229–2240.

Jia, G., S. Bai, Y. Lin, et al. 2023. "Representation of Conspecific Vocalizations in Amygdala of Awake Marmosets." *National Science Review* 10, no. 11: nwad194.

Kandel, E. R. 2013. *Principles of Neural Science*. 5th ed. McGraw Hill Professional.

Klempin, F., G. Kronenberg, G. Cheung, H. Kettenmann, and G. Kempermann. 2011. "Properties of Doublecortin-(DCX)-Expressing Cells in the Piriform Cortex Compared to the Neurogenic Dentate Gyrus of Adult Mice." *PLoS ONE* 6, no. 10: e25760.

La Rosa, C., F. Cavallo, A. Pecora, et al. 2020. "Phylogenetic Variation in Cortical Layer II Immature Neuron Reservoir of Mammals." *Elife* 9, no. July: e55456.

Liu, C., C. C.-C. Yen, D. Szczupak, X. Tian, D. Glen, and A. C. Silva. 2021. "Marmoset Brain Mapping V3: Population Multi-Modal Standard Volumetric and Surface-Based Templates." *Neuroimage* 226, no. February: 117620.

Li, Y.-N., D.-D. Hu, X.-L. Cai, et al. 2023. "Doublecortin-Expressing Neurons in Human Cerebral Cortex Layer II and Amygdala From Infancy to 100 Years Old." *Molecular Neurobiology* 60, no. 6: 3464–3485.

Lockard, B. I. 1985. "The Forebrain of the Ferret." *Laboratory Animal Science* 35, no. 3: 216–228.

Lois, C., J. M. García-Verdugo, and A. Alvarez-Buylla. 1996. "Chain Migration of Neuronal Precursors." *Science (New York, NY)* 271, no. 5251: 978–981.

Luzzati, F., L. Bonfanti, A. Fasolo, and P. Peretto. 2009. "DCX and PSA-NCAM Expression Identifies a Population of Neurons Preferentially Distributed in Associative Areas of Different Pallial Derivatives and Vertebrate Species." *Cerebral Cortex (New York, NY: 1991)* 19, no. 5: 1028–1041.

Luzzati, F., P. Peretto, P. Aimar, G. Ponti, A. Fasolo, and L. Bonfanti. 2003. "Glia-Independent Chains of Neuroblasts Through the Subcortical Parenchyma of the Adult Rabbit Brain." *Proceedings of the National Academy of Sciences of the United States of America* 100, no. 22: 13036–13041.

Marlatt, M. W., I. Philippens, E. Manders, et al. 2011. "Distinct Structural Plasticity in the Hippocampus and Amygdala of the Middle-Aged Common Marmoset (*Callithrix jacchus*)." *Experimental Neurology* 230, no. 2: 291–301.

Martí-Mengual, U., E. Varea, C. Crespo, J. M. Blasco-Ibáñez, and J. Nacher. 2013. "Cells Expressing Markers of Immature Neurons in the Amygdala of Adult Humans." *European Journal of Neuroscience* 37, no. 1: 10–22.

Mcconnell, J., and J. B. Angevine Jr.. 1983. "Time of Neuron Origin in the Amygdaloid Complex of the Mouse." *Brain Research* 272, no. 1: 150–156.

Mizukawa, K., I. M. Tseng, and N. Otsuka. 1989. "Quantitative Electron Microscopic Analysis of Postnatal Development of Zinc-Positive Nerve Endings in the Rat Amygdala Using Timm's Sulphide Silver Technique." *Brain Research Developmental Brain Research* 50, no. 2: 197–203.

Mulc, D., D. Smilović, Ž. Krsnik, et al. 2024. "Fetal Development of the Human Amygdala." *Journal of Comparative Neurology* 532, no. 1: e25580.

Murray, E. A., and L. K. Fellows. 2022. "Prefrontal Cortex Interactions With the Amygdala in Primates." *Neuropsychopharmacology: Official Publication of the American College of Neuropsychopharmacology* 47, no. 1: 163–179.

Myers, P., R. Espinosa, C. S. Parr, T. Jones, G. S. Hammond, and T. A. Dewey. 2019. *The Animal Diversity Web*. https://animaldiversity.org.

Nacher, J., E. Lanuza, and B. S. McEwen. 2002. "Distribution of PSA-NCAM Expression in the Amygdala of the Adult Rat." *Neuroscience* 113, no. 3: 479–484.

Page, C. E., S. W. Biagiotti, P. J. Alderman, and S. F. Sorrells. 2022. "Immature Excitatory Neurons in the Amygdala Come of Age During Puberty." *Developmental Cognitive Neuroscience* 56, no. August: 101133.

Pattaro, A., M. Ghibaudi, C. Corrente, et al. 2025. "Phylogenetic Variation of Layer II Cortical Immature Neurons in Dog and Horse Confirms Covariance With Brain Size and Neocortical Surface." *Brain Structure & Function* 230, no. 6: 115.

Piumatti, M., O. Palazzo, C. La Rosa, et al. 2018. "Non-Newly Generated, 'Immature' Neurons in the Sheep Brain Are Not Restricted to Cerebral Cortex." *Journal of Neuroscience: The Official Journal of the Society for Neuroscience* 38, no. 4: 826–842.

Quah, S. K. L., L. McIver, A. C. Roberts, and A. M. Santangelo. 2020. "Trait Anxiety Mediated by Amygdala Serotonin Transporter in the Common Marmoset." *Journal of Neuroscience: The Official Journal of the Society for Neuroscience* 40, no. 24: 4739–4749.

Radtke-Schuller, S. 2018. *Cyto- and Myeloarchitectural Brain Atlas of the Ferret (Mustela putorius) in MRI Aided Stereotaxic Coordinates*. Springer.

Remedios, R., D. Huilgol, B. Saha, et al. 2007. "A Stream of Cells Migrating From the Caudal Telencephalon Reveals a Link Between the Amygdala and Neocortex." *Nature Neuroscience* 10, no. 9: 1141–1150.

Rotheneichner, P., M. Belles, B. Benedetti, et al. 2018. "Cellular Plasticity in the Adult Murine Piriform Cortex: Continuous Maturation of Dormant Precursors into Excitatory Neurons." *Cerebral Cortex (New York, NY: 1991)* 28, no. 7: 2610–2621.

Sawada, K., and M. Watanabe. 2012. "Development of Cerebral Sulci and Gyri in Ferrets (*Mustela putorius*)." *Congenital Anomalies* 52, no. 3: 168–175.

Sawiak, S. J., Y. Shiba, L. Oikonomidis, et al. 2018. "Trajectories and Milestones of Cortical and Subcortical Development of the Marmoset Brain from Infancy to Adulthood." *Cerebral Cortex* 28, no. 12: 4440–4453.

Schultz-Darken, N., K. M. Braun, and M. E. Emborg. 2016. "Neurobehavioral Development of Common Marmoset Monkeys." *Developmental Psychobiology* 58, no. 2: 141–158.

Shapiro, L. A., K. Ng, Q.-Y. Zhou, and C. E. Ribak. 2009. "Subventricular Zone-Derived, Newly Generated Neurons Populate Several Olfactory and Limbic Forebrain Regions." *Epilepsy & Behavior: E&B* 14, no. S1: 74–80.

Soma, M., H. Aizawa, Y. Ito, et al. 2009. "Development of the Mouse Amygdala as Revealed by Enhanced Green Fluorescent Protein Gene Transfer by Means of in Utero Electroporation." *Journal of Comparative Neurology* 513, no. 1: 113–128.

Song, H., C. F. Stevens, and F. H. Gage. 2002. "Astroglia Induce Neurogenesis From Adult Neural Stem Cells." *Nature* 417, no. 6884: 39–44.

Sorrells, S. F., M. F. Paredes, D. Velmeshev, et al. 2019. "Immature Excitatory Neurons Develop During Adolescence in the Human Amygdala." *Nature Communications* 10, no. 1: 2748.

Takamori, Y., T. Wakabayashi, T. Mori, J. Kosaka, and H. Yamada. 2014. "Organization and Cellular Arrangement of Two Neurogenic Regions in the Adult Ferret (*Mustela putorius furo*) Brain." *Journal of Comparative Neurology* 522, no. 8: 1818–1838.

Varea, E., M. Belles, S. Vidueira, et al. 2011. "PSA-NCAM Is Expressed in Immature, but Not Recently Generated, Neurons in the Adult Cat Cerebral Cortex Layer II." *Frontiers in Neuroscience* 5, no. February: 17.

Xiong, K., D.-W. Luo, P. R. Patrylo, et al. 2008. "Doublecortin-Expressing Cells Are Present in Layer II Across the Adult Guinea Pig Cerebral Cortex: Partial Colocalization With Mature Interneuron Markers." *Experimental Neurology* 211, no. 1: 271–282.

Zhang, X.-M., Y. Cai, Y. Chu, et al. 2009. "Doublecortin-Expressing Cells Persist in the Associative Cerebral Cortex and Amygdala in Aged Nonhuman Primates." *Frontiers in Neuroanatomy* 3, no. October: 17.

Zhu, L., D. Zheng, R. Li, et al. 2023. "Induction of Anxiety-Like Phenotypes by Knockdown of Cannabinoid Type-1 Receptors in the Amygdala of Marmosets." *Neuroscience Bulletin* 39, no. 11: 1669–1682.

Supporting Information

Additional supporting information can be found online in the Supporting Information section.

Figure S1 Age comparison across species. To enable comparisons among mammals with widely different lifespans, the average period

before reproductive maturity (cyan bar) and the average lifespan (black bar) were considered across species. Data were obtained from AnAge and Animal Diversity Web, comprehensive databases of animal natural and life history, aging, distribution, classification, and conservation biology (de Magalhães and Costa 2009; Myers et al. 2019). Purple arrows indicate the ages considered in this study. **Supporting Information**: cne70155-sup-0002-MovieS1.avi